AD-A047 739 MASSACHUSETTS INST OF TECH CAMBRIDGE AEROPHYSICS LAB F/G 4/1
WIND TUNNEL TESTS OF THE UPSTREAM INFLUENCE OF A CONICAL MASS S--ETC(U)
SEP 77 C W HALDE, R A KRAEMER, B ZIPH F19628-76-C-0185

UNCLASSIFIED MIT-TR-197 AFGL-TR-77-0210 NL

| OF |

AD
A047 739

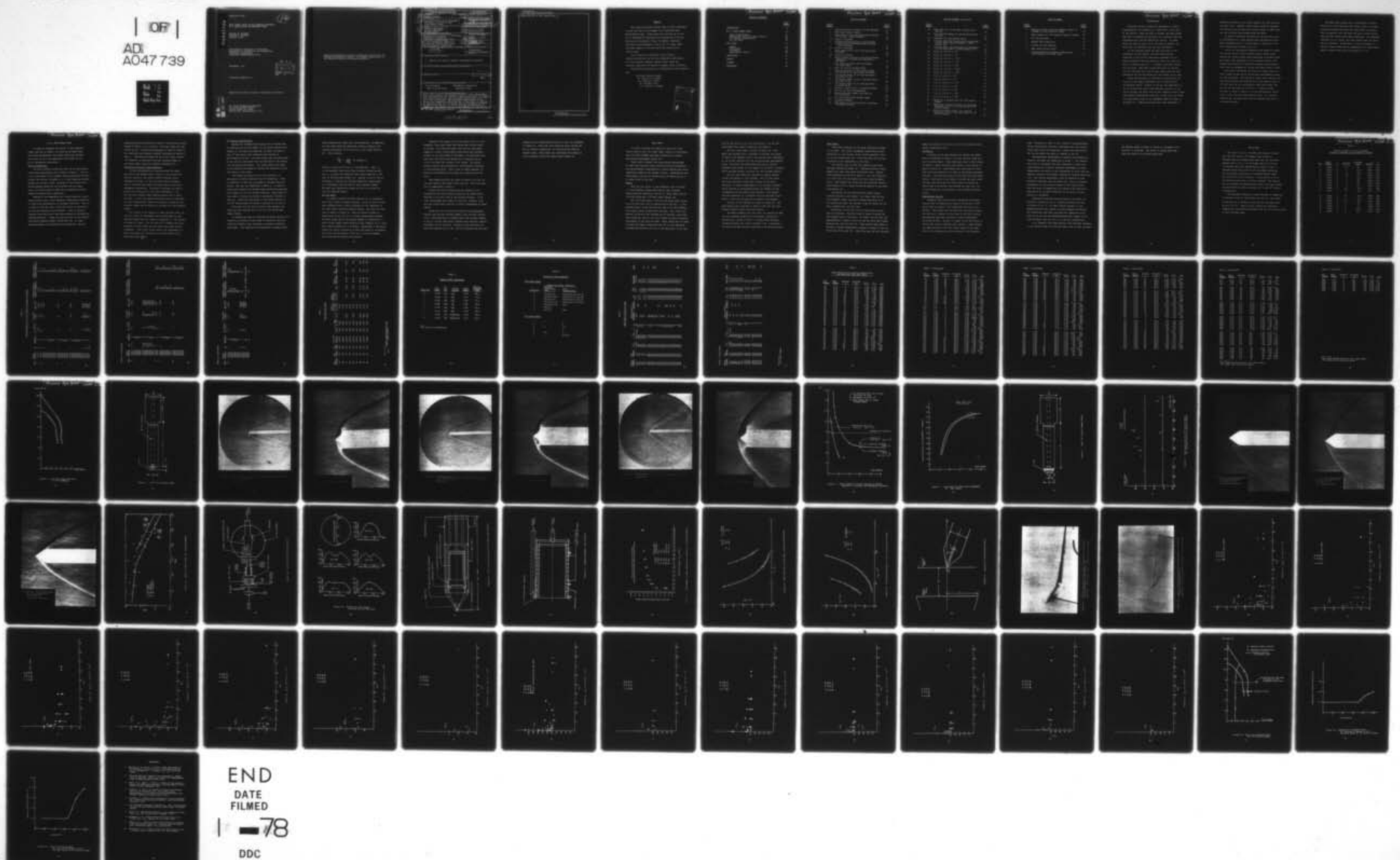

END
DATE
FILMED
1 -78
DDC

AD A047739

AFGL-TR-77-0210

12

WIND TUNNEL TESTS OF THE UPSTREAM INFLUENCE OF A CONICAL MASS SPECTROMETER PROBE

Charles W. Haldeman
Richard A. Kraemer
Benjamin Ziph

Massachusetts Institute of Technology
Department of Aeronautics and Astronautics
Aerophysics Laboratory
Cambridge, Massachusetts 02139

September, 1977

Scientific Report No. 1

Air Force Geophysics Laboratory
Air Force Systems Command
United States Air Force
Hanscom AFB, Massachusetts 01731

19

REPORT DOCUMENTATION PAGE

READ INSTRUCTIONS BEFORE COMPLETING FORM

1. REPORT NUMBER: 18 AFGL-TR-77-0210	2. GOVT ACCESSION NO.
3. RECIPIENT'S CATALOG NUMBER: 9 Rept. for	
4. TITLE (and Subtitle): 6 Wind Tunnel Tests of the Upstream Influence of a Conical Mass Spectrometer Probe.	5. ~~TYPE OF REPORT & PERIOD COVERED~~ ~~Scientific Report No. 1~~ 1 Apr 76 - 31 Aug 77
	6. PERFORMING ORG. REPORT NUMBER: 14 MIT-TR-197, SCIENTIFIC-1
7. AUTHOR(s): 10 Charles W. Haldeman, Richard A. Kraemer, Benjamin Ziph	8. CONTRACT OR GRANT NUMBER(s): 15 F19628-76-C-0185 New
9. PERFORMING ORGANIZATION NAME AND ADDRESS: Massachusetts Institute of Technology, Aerophysics Laboratory, Cambridge, Massachusetts 02139	10. PROGRAM ELEMENT, PROJECT, TASK AREA & WORK UNIT NUMBERS: 16 61102F 86051101 17 11
11. CONTROLLING OFFICE NAME AND ADDRESS: Air Force Geophysics Laboratory, Hanscom AFB, Massachusetts 01731, Monitor/Edmund A. Murphy/LKD	12. REPORT DATE: 11 Sept~~ember,~~ 1977
	13. NUMBER OF PAGES: 88
14. MONITORING AGENCY NAME & ADDRESS (if different from Controlling Office): 12 83p.	15. SECURITY CLASS. (of this report): Unclassified
	15a. DECLASSIFICATION/DOWNGRADING SCHEDULE

16. DISTRIBUTION STATEMENT (of this Report)

A - Approved for public release; distribution unlimited.

17. DISTRIBUTION STATEMENT (of the abstract entered in Block 20, if different from Report)

18. SUPPLEMENTARY NOTES

19. KEY WORDS (Continue on reverse side if necessary and identify by block number)

Ground Testing
High Altitude Probe
Atmospheric Composition
Supersonic Flow

20. ABSTRACT (Continue on reverse side if necessary and identify by block number)

Wind tunnel tests of two configurations of a mass spectrometer high altitude probe are reported. Results show that a 35 degree half angle conical nose has an attached shock wave at M=3 from 25 to 100 km altitude. Spectrographic measurements of the density and temperature perturbations at the probe tip indicate no influence below 70 km altitude with an increasing influence between 70 and 100 km. At 100 km altitude perturbations of temperature and density are still much smaller for the conical

over

009 200 LB

probe than for a flat faced probe.

PREFACE

This report describes studies made of shock attachment at high altitude to the skimmer of an aspirated mass spectrometer probe. These tests were carried out at the M.I.T. Aerophysics Laboratory wind tunnels and at Arnold Engineering Development Center, Tullahoma, Tennessee. Particular acknowledgment is due to Dr. T. Dwayne McKay and other members of the ARO staff who conducted the latter tests.

This research was supported under Contract F19628-76-C-0185 by the Air Force Geophysics Laboratory, Air Force Systems Command, Hanscom Field, under the Technical Cognizance of Edmund A. Murphy, Contract Monitor.

Professional personnel who contributed to this research are:

Professor Morton Finston
Dr. Charles W. Haldeman
Mr. Charles E. Hawks
Mr. Benjamin Ziph
Mr. Richard A. Kraemer

Preceding Page Blank - Filmed

TABLE OF CONTENTS

PRECEDING PAGE BLANK - NOT FILMED

LIST OF FIGURES

LIST OF FIGURES (continued)

LIST OF TABLES

Preceding Page Blank - NOT FILMED

INTRODUCTION

Supersonic flight through the atmosphere is always accompanied by the formation of a shock wave at the nose of the vehicle. When the body is slender and sharp nosed, this wave is attached to the point at an oblique angle and propagates away from and behind the vehicle. In cases where the body is blunt (1) or the nose is rounded, the shock wave is displaced from the nose (detached).

At low altitudes where the mean free path in the atmosphere is much smaller than the characteristic dimension of the pointed nose, shock attachment can be easily predicted from the classical flow of an ideal gas about an infinite cone (2). At higher altitudes, however, the continuum flow model breaks down until at extreme altitude the mean free path is much larger than the body dimensions and the free molecular flow theory can be used.

Shock wave position is important in determining the state of a gas sample aspirated into an airborne mass spectrometer probe. Because of heating and compression in the shock wave and finite rate chemical reactions in the region between the shock wave and the sampling orifice, mass spectrometer measurements from such a probe will not reveal the unperturbed state of the atmosphere when the shock is detached (3). Numerical methods have been developed to simulate reactions in the region between the shock wave and the nose (4,5). However, these require accurate knowledge of reaction rates and particle energies which in some cases are the variables being measured by the probe.

In order to minimize the effect of the bow shock wave on measurements by a nose mounted mass spectrometer probe, AFGL considered use of a conical probe in addition to the blunt faced probe already in use (1).

The M.I.T. Aerophysics Laboratory was asked to conduct wind tunnel tests of this proposed conical faced probe. Because the initial probe design exhibited a detached shock wave under test conditions at low altitude and M=4, this program was directed to testing an improved configuration. Later this was extended to include full-scale tests at AEDC.

This report describes the results of these tests and their impact on the use of conical mass spectrometer probes at high altitudes. The results of these tests indicate that the shock wave will be attached to a clean conical nose of 35° half angle at the anticipated flight Mach number near M=3 for all altitudes up to 100 km. A typical flight corridor is shown in Figure 1 for the UTE-Tomahawk vehicle used to carry the mass spectrometer probe. At altitudes below 60 km, the shock wave will be attached above M=1.71, the lowest tested.

The AEDC tests showed that at the higher altitudes, 80-100 km in the transition flow regime, there is a small upstream influence even when the shock wave is attached. This is expected since the mean free path is much larger than the nose radius under these conditions. The upstream influence is, of course, very much greater when the shock wave is detached. Specifically, at M=3 the density is thirteen times higher and the temperature 2.8 times higher behind a normal shock wave than ahead of it (2).

Preceding Page Blank - Filmed

M.I.T. WIND TUNNEL TESTS

In order to determine the region of the proposed flight corridor of Figure 1 in which an attached shock wave could be expected, wind tunnel tests were carried out in the 18 x 24 inch supersonic wind tunnel at the M.I.T. Aerophysics Laboratory.

Blunt Configuration

The first geometry tested was that for the anticipated flight mass spectrometer and is shown in Figure 2. This is a 1/10 scale model of the skimmer (AFCRL Drawing LKD 73-6912) without the orifice, attached to a .9 inch diameter cylinder. Because of the small scale, inclusion of the orifice and a vacuum pumping system was not practical for the tests. Later, full scale tests at AEDC with an aspirated orifice showed no effects due to aspiration.

Because of the combination of a blunt nose and a short sharp conical point in this geometry, theoretical prediction of shock wave configuration is extremely difficult. This is a result of the fact that a shock wave which is attached at the tip will impinge on the shoulder. This can cause an unstable shock wave which oscillates between an attached and detached position. Indeed this was the case at $Re=.138\times10^6$, the highest Reynolds number tested with $M=4$. At lower Reynolds numbers no oscillations were observed. The two appropriate shock positions are shown in the Schlieren photographs of Figure 3, 3a, 4 and 4a. The blunt model was also tested at M=2. A Schlieren photograph is shown in Figure 5. Run conditions and measured standoff distances are given in Table 1. Tabulated altitudes are for a full scale vehicle (9" diameter) to experience the test Reynolds number at test Mach number using the standard atmosphere (6).

Theoretical Limits on Shock Position

A brief investigation of available data for shock position on the skimmer model (Figure 2) was carried out. Data was found for the shock standoff distance from a hemisphere cylinder (7) and from blunt-faced cylinders used in previous wind tunnel blocking tests at the M.I.T. Aerophysics Laboratory. This data is plotted in Figure 6 along with the results of the tests from Table 1. At M=2 the blunt skimmer model behaves exactly like a blunt cylinder. At M=4 the complex oscillation sets in and there are three experimental results--one which is stable at low Reynolds number and two which are bi-stable at high Reynolds number.

For a model in the shape of a right circular cone, the cone half angle for detachment can be calculated at high Reynolds number from the tables of Reference 2. The results are shown in Figure 7 for $\alpha=0$ and $\alpha=25^{\circ}$, assuming the axial component of Mach number and the local cone angle control attachment. This figure shows clearly the advantages of a small cone angle for providing an attached shock at low supersonic Mach number.

35° Conical Configuration

Because the attached shock region did not extend down to sufficiently low Mach number for the blunt configuration (Figure 2), the model was modified, as shown in Figure 8. This 35° half angle nose reproduced the contours of AFGL Drawing C-76-702. One small groove near the mid-length of the cone was associated with the junction of the skimmer with the mass spectrometer. The larger groove just ahead of the shoulder was needed to connect the protective shield used early in the flight.

This model was tested at M=3, M=2 and M=1.71 at equivalent altitudes between 25 and 67 kilometers. Under no condition of test was a detached or unstable shock observed. The data are summarized in Table 2. At angle of attack both windward and leeward shock angles were measured with respect to the free stream direction. Shock angle at zero angle of attack is plotted vs equivalent altitude in Figure 9. Schlieren photographs of the shock position on the 35° conical model are shown in Figures 10, 11 and 12.

Note that with the purely conical nose geometry the shock wave was attached even at M=1.71, the lowest Mach number tested.

An attempt was made to calculate the shock position as a function of altitude at zero angle of attack by using the classical boundary layer thickness to provide a modified body shape. This approach was unsuccessful, yielding shock angle changes much larger than those observed. An empirical fit was found using the analytical form but choosing the constant multiplier to fit the M.I.T. wind tunnel data for M=3. This relation

$$\frac{d\Theta_s}{\Theta_s} = \frac{4.6}{\sqrt{Re_d}} \text{ is plotted in}$$

Figure 13 along with the M.I.T. and AEDC data. Here Θ_s is the measured shock angle from the model centerline and $d\Theta_s$ is Θ_s minus the tabulated ideal shock angle for a 35° cone at the test Mach number (2). Scatter is due to the uncertainty in drawing and visually measuring a shock angle on a photograph, particularly at lower Reynolds number. The AEDC data indicate the trend for $d\Theta/\Theta$ to roll-off at very low Reynolds number.

Arc Jet Tests

In order to extend the data from the M.I.T. supersonic wind tunnel tests to higher altitude, a short series of tests were conducted using a small nitrogen arc jet connected to the wind tunnel auxiliary pumping system. The setup for this test is shown in Figure 14. Here arc heated nitrogen is supplied by an arc jet (8) to a water cooled plenum chamber. The down stream end of the plenum chamber is connected to a water cooled copper nozzle having an exit diameter of 3.1 inch and a throat diameter of 0.9 inches. Downstream of the throat region the nozzle diverges at a cone half angle of 15 degrees. The nozzle exited forming a free jet in the test chamber, which enclosed both model and diffuser.

Because of the small size of the nozzle, the 0.75 inch diameter (.083 scale) model was tested only at zero angle of attack. Five runs were made, the flow for each being mapped by a water cooled impact probe which was traversed across the jet just ahead of the model. To facilitate this both model and probe were mounted on a rotatable arm so one or the other was located in the stream. An angular position signal was developed by a potentiometer connected to the mounting shaft. Thus a plot of impact pressure vs position was obtained as the probe was rotated across the flow.

Mach number profiles are shown in Figure 15 as well as the path taken by the probe across the jet. Data from these runs is summarized in Table 3.

During all runs the shock wave was observed to be attached but was only faintly visible to the naked eye as observed in the self glow of the excited nitrogen. 35 mm color photographs were taken for each run. However, they were not sufficiently distinct to permit measurement of shock angles.

These runs are of value even without this measurement because they provide low Mach number, high altitude information. From these tests it appears that even at Mach numbers as low as 1.8 the shock wave (although very diffuse), remains attached at 85 km altitude. Because of the relatively low mass flow through the arc jet, the arc stability was not good, leading to the inconsistency from run to run, as evidenced in Figure 15. Since the pitot probe was water cooled and was at constant temperature, no correction was made for thermal creep. Mach number was calculated from impact to static pressure ratios and normal shock tables (2).

AEDC TESTS

In order to verify the results of the M.I.T. wind tunnel tests on the 1/10 scale model, tests of a full-scale and 1/10 scale skimmer nose were carried out at Arnold Engineering Development Center (9).

These tests included flow visualization photographs of shock wave position using electron excited fluorescence and spectrographic measurements of static density and static temperature ahead of the skimmer orifice. Measurements were made between -20 and +20 degrees angle of attack and up to 8 inches ahead of the nose.

Models

Both the full scale (9 inch diameter) and 1/10 scale (.9 inch diameter) models were made of 6061 aluminum duplicating the geometry of the M.I.T. tests (AFGL Drawing C-76-702) which was a 35° half angle conical tip.

The 1/10 scale model, like the 1/10 scale model tested at M.I.T., was solid with no aspiration at the tip. It was machined from a solid aluminum bar with a 3/8 inch diameter hard copper insert pressed into the nose. This insert was machined along with the aluminum bar to provide a very high heat conduction rate at the tip in order to survive possible impingement of the electron beam. Model length was 15 inches to match the support mechanism with its 15 inch extension installed and position the tip at the same point in the test flow as the point of the full-scale model. For the full scale model this support extension was removed.

The full scale model is shown in Figure 16. This model was equipped with a cryopump to evacuate the region in back of the skimmer orifice and provide exact simulation of the flight condition for the aspirated mass spectrometer probe. The model was constructed entirely of 6061-T6 aluminum alloy except for the copper tip and Kel-F insulator, which provided thermal isolation for the cryopump section.

Two 3/4 inch tubes were provided to supply gaseous helium refrigerant to the cryopump. Two 1/2 inch tubes were also provided, welded just forward of the Kel-F insulator, to permit measurement of the internal pressure and to provide an outgassing channel for removal of the cryodeposit from the pump during bakeout. This bakeout line was connected to a solenoid valve at the base of the model to vent the cryopump during bakeout and pumpdown.

Details of the cryopump are shown in Figure 17. Two band heaters were provided as shown to bake off the cryodeposit between tunnel operating periods.

The model assembly was leak tight, as received at AEDC and the cryopump operated as anticipated, consistently maintaining a vacuum of below .1 stream static pressure. Cryopump pressure was usually between 0 and .1 millitorr, as read by the MKS Baratron connected to the metering port.

Wind Tunnel

Tests were conducted in the space simulation chamber 10v at AEDC. This large cryopumped vacuum facility was connected to a M=3 conical nozzle, which provided a free jet in the vacuum tank (10). Flow from this jet was then collected on the cryobaffles in the tank.

Calibration runs at each test condition were made and were reported by McKay (9). Tabulated values of Mach number were taken from these calibration runs. Nominal flow conditions are given in Table 4. For flow conditions 6, 7 and 8 the flow was merged with the nozzle boundary layer. Mach numbers for these runs are therefore approximate because of the viscous correction applied to the probe measurements (9).

Conditions 2-6 were obtained with normal liquid nitrogen cooling in the nozzle. For these runs the core flow diameter, where the pitot pressure was above .9 of the centerline value, was between 15 and 12 inches and the axial gradient was .016 per inch.

Conditions 7 and 8 were run with the nozzle cooled only by radiation. They were made in order to extend the Mach number range of the data. For these runs the core was approximately 8 inches in diameter and the axial Mach number gradient was .021 per inch (9). Test section Mach number is plotted vs plenum (stagnation) pressure in Figure 18 for the conditions of the test (9). Mean free path and unit Reynolds number are plotted in Figures 19 and 20 from earlier wind tunnel calibrations (10).

Run Matrix

A listing of the data obtained at various run conditions is presented in Table 5 for both the full scale and the 1/10 scale model. Flow conditions refer to the listing in Table 4. Model location with respect to the nozzle is shown in Figure 21. Both models were positioned so their nose tips were located at 0-0 when at the maximum upstream position. Data was then taken as the model was moved downstream. Thus data at zero angle of attack was taken along the body axis while data at other angles of attack was taken along a horizontal line through the nose tip; i.e., a line through the tip parallel to the oncoming velocity vector.

Experimental Results

Measured shock wave position determined from photographic data is summarized in Table 6 and values of $d\Theta/\Theta$ are plotted in Figure 13 for comparison with the M.I.T. results. This shows that the empirical correlation found for the M.I.T. results is also close to the AEDC results. Measurements were made directly on glossy photographs furnished by AEDC. Scatter is caused by the difficulty in fitting the curved, diffused shock exactly. These showed the lower portion of the flow region ahead of the model nose in the recombination glow produced by the electron beam. Vacancies in Table 6 are a result of the photographs having insufficient contrast to delineate the high density shock region from the background. Sample data photographs for the two models are shown in Figures 22 and 23.

Spectrographic measurements of density and temperature ahead of the model are summarized in Table 7. The temperature data is considered the best indication of local flow state because the relative intensity measurement on which temperatures are based is less susceptible to noise than the absolute intensity measurement required for density determination. The density measurement could be effected by back scattered electrons from the model nose. This is probably responsible for the greater scatter in the density data. Thus the point of temperature rise ahead of the vehicle is believed to be the best indication of the point at which density is increased.

Temperature profiles directly ahead of the model are plotted in Figures 24 to 30. Density profiles are given in Figures 31 to 37. In these figures distance is non-dimensionalized with respect to probe diameter and density and temperature have been corrected for temperature drift from run to run and non-dimensionalized with respect to the value farthest from the tip; i.e., the free stream value.

It is apparent from these profiles that upstream influence of the conical probe is relatively small even at high altitudes and becomes larger as angle of attack is increased or as altitude is increased. The effect is always much less than the effect of a detached shock wave.

CONCLUSIONS

The tests at M.I.T. and AEDC wind tunnels indicate that the full conical 35° skimmer nose, Figure 8, operates with an attached shock wave over all test Mach numbers from 1.71 to 3 at altitudes from 26 to 103 km. In contrast the blunt configuration, Figure 2, has a detached shock wave at M=2 at all altitudes tested and has an unstable alternating (attached-detached) shock wave at M=4 and 40 km altitude. At M=4 and 45 to 65 km altitude the shock wave is stably attached. The regions for an attached and detached shock wave in the Mach number altitude plane are shown in Figure 38 for the 35° conical configuration.

The upstream influence at high altitudes is summarized in Figures 39 and 40, which show T/T_∞ and ρ/ρ_∞ just ahead of the nose as a function of altitude for the AEDC tests at M=3.2 to 3.7. These provide a basis for correcting temperatures and densities measured with the 35° conical probe in this altitude range.

PrecedING Page BLank - NOT FiLMed

Table 1

Results of Tests of First Geometry
(Figure 2) Skimmer at Zero Angle of Attack

Run	Photo Number	M	p_o (psia)	Altitude (km)	$Rex10^{-6}$	$\frac{\Delta}{R}$
A	65009	4	4.8	50	.035	.584
A	65010	4	1	62.5	.0072	.584
A	65011	4	.7	65.5	.005	.584
A	65013	4	1.8	58	.0128	.584
A	65014	4	3	53.5	.0212	.584
A	65015	4	6	48	.0416	.604
A	65016	4	9	45	.0621	.604
A	65019	4	9	45	.0620	.604
A	65020	4	20	39.5	.138	.566
A	65021	4	20	39.5	.138	.510
B	65025	2	4.5	35.5	.0827	.904
B	65027	2	1	45.5	.0187	.892
B	65028	2	1.8	41.5	.0335	.892
B	65031	2	3	38	.0551	.892
B	65032	2	6	34	.1089	.892
B	65034	2	9	30.5	.1640	.892
B	65040	2	15	27.5	.2621	.892

Table 2

Shock Angles on a 35^{o} Conical (Figure 8) Model

Run	Photo Number	M	α Degrees	P_o (psia)	Altitude (km)	Rex 10^{-6}	Windward Shock Angle (Degrees)	Leeward Shock Angle (Degrees)
1	65047	2	0	3.85	36	.0745	56.5	57
2	65048	2	0	15	27.7	.2756	55.5	55.5
3	65049	2	0	6	34	.1102	59	57.5
	65050		0				57	57
	65051		5				56	57
	65052		10				58	59
	65053		15				61	63
	65054		20				63.5	66
	65055		25				60	68.5
	65056		0				57	58
4	65057	2	0	2	41	.0367	60	59
	65058		5				60	66.5
	65059		10				63	66
	65060		15				63.5	64
	65061		20				64	71
	65062		25				60.5	74
	65063		0				61	61
5	65064	2	0	.8	45.5	.0147	58.5	58.5
	65065		5				61	63.5
	65066		10				62.5	63.5
	65067		15				63.5	63
	65068		20				73	75
	65069		25					
	65070		0				59	59
	65071	2	0	.7	49	.0129	63	59
	65072	2	0	.61	49.5	.0112	61	61.5
	65073	2	0	.6	49.5	.0110	63	61
	65074	2	0	.58	50	.0107	60	60
	65075	1.71	0	3.5	35	.0714	60	60

Table 2 (continued)

Run	Photo Number	M	α Degrees	p_o (psia)	Altitude (km)	Rex 10^{-6}	Windward Shock Angle (Degrees)	Leeward Shock Angle (Degrees)
6	65076	1.71	0	15	25.7	.3060		
	65077		5					
	65078		10					
	65079		15					
	65080		20					
	65081		0					
7	65082	1.71	0	6	31.5	.1224		
	65083	1.71	0	3	36	.0612		
	65084	1.71	0	1	43	.0204		
	65085	1.71	0	.8	45	.0163		
	65086	1.71	10	.6	47	.0122		
	65087	1.71	25	.6	47	.0122		
	65088	3	0	5.25	41.8	.0643		
8	65089	3	0	20	39.8	.225	46	46
	65090		0				45.5	45.5
9	65091	3	0	6	41.3	.0675	47	46
	65092		5				46	47
	65093		10				46	47.5
	65094		15				47.5	49
	65095		20				49	51
	65096		25				50	55
	65097		0				46.5	47
10	65098	3	0	2	48.2	.0228	47	47.5
	65099		5				46	47.5
	65100		10				48	48
	65101		15				48	50
	65102		20				48	51
	65103		25				50	54.5
	65104		0				47	47

Table 2 (continued)

Run	Photo Number	M	Degrees	p_o (psia)	Altitude (km)	Rex 10^{-6}	Windward Shock Angle (Degrees)	Leeward Shock Angle (Degrees)
11	65105	3	0	.8	56	.0182	48	47.5
	65106		5				48.5	48.5
	65107		10				47.5	49
	65108		15				50.5	51
	65109		20				50.5	52
	65110		25				49	57
	65111		0				48	49
	65112	3		.7	57.5	.00814		
	65113	3	0	.6	58.5	.00697	48	47
	65114	3		.5	60	.00581		
	65115	3	10	.5	60	.00581	Shock is not visible near nose	
	65116							
	65117		25				56	62

Table 3

Arc Jet Test Data

Run Number	Arc Volts	Arc Amps	N_2 Flow lb/sec	η_{Arc}*	H_o $\frac{Btu}{lb}$	T_o ^oK	Static Pressure P_s torr	Impact Pressure P_i torr	M	Equiv. Altitude	Re Model	Re Nozzle
1a	45	185	.00123	.468	3006		0.40					
1b	20	240	.00123	.129	4760		0.40					
1c	50	138	.00123	.434	2306	3500	0.40	4.30	2.83	76 Km	653	2773
2a	60	110	.00178	.489	1716		0.50					
2b	50	140	.00178	.518	1929	3200	0.50	2.40	1.83	84 Km	123	521
3a	40	170	.00135	.420	2011		0.54					
3b	50	140	.00135	.453	2229	3500	0.55	2.45	1.75	85 Km	106	450
4a	50	220	.00134	.478	3714	4000	0.47	2.57	1.97	85 Km	111	474
5a	42	235	.00090	.334	3469	3900	0.50	3.60	2.29	81 Km	234	992

* $\eta_{Arc} = \frac{\text{Input Power-Cooling Loss}}{\text{Input Power}}$

Table 4

Nominal Test Conditions

Condition	p_o (torr)	T_o (^oK)	Nozzle Cooling	Mach Number	Density Altitude (Km)
1*	1.500	270	LN_2	3.75	69.5
2	1.000	275	LN_2	3.71	72.5
3	0.450	280	LN_2	3.64	77.5
4	0.400	840	LN_2	3.60	84.5
5	0.150	290	LN_2	3.49	83.0
6	0.150	865	LN_2	3.45	89.0
7	0.100	300	Radiation	3.20	84.5
8	0.100	840	Radiation	3.16	89.5

*Run only for calibration.

Table 5

Listing of Data Acquired

Full-Scale Model

	Angles of Attack (degrees)	
Condition	Density Temperature Data	Flow Visualization
2	20,10,0,-10	20,10,5,0,-5,-10,-20
3	20,10,5,0,-10	20,10,5,0,-5,-10,-20
4	20,10,0,-10	20,10,5,0,-5,-10,-20
5	20,10,5,0,-10	20,10,5,0,-5,-10,-20
6	20,10,5,0,-10	20,0
7	20,10,0	
8	20,10,0	20,0

1/10 Scale Model

2	5	5
3		5
4	5	5,0
5		5
6	5,0	5
7	5	20,10,5

Table 6

AEDC Shock Position Data

Photo Number	Run Number	T_o	P_o	α	Shock Angle Θ Windward	Shock Angle Θ Leeward	M	Re_d	Altitude	$d\Theta/\Theta$
311	19	269^oK	1000 mtorr	20^o	48^o		3.71	1715	72.5 km	
317	25	269	1000	-20		49^o	3.71		72.5	
312	20	269	1000	10	53		3.71	1715	72.5	
316	24	269	1000	-10	59			1715	72.5	
314	22	269	1000	0	54		3.71	1715	72.5	.25
315	23	269	1000	-5		54	3.71	1715	72.5	
606	289	269	100	0	56		3.20	223	83.5	.25
607	290	269	100	20	49		3.20	223	83.5	
608	291	836	400	20	65		3.60	155	84.5	
609	292	836	400	0	.49		3.60	155	84.5	.13
610	293	836	400	0	53		3.60	155	84.5	.22
611	294	836	400	5	50		3.60	155	84.5	
616	299	836	400	-5		64	3.60	155	84.5	
612	295	836	400	10	62		3.60	155	84.5	
615	298	836	400	10	66		3.60	155	84.5	
613	296	836	400	20	49		3.60	155	84.5	
614	297	836	400	-20		63	3.60	155	84.5	
617	349	367	450	-20		65	3.64	523	79.5	
623	355	336	450	20	52		3.64	591	79.0	
618	350	362	450	-10		58	3.64	533	79.5	
622	354	344	450	-10	51		3.64	572	79.0	
619	351	358	450	-5		54	3.64	541	79.5	
621	353	349	450	5	51		3.64	561	79.0	
620	352	354	450	0	55		3.64	550	79.5	.26
624	356	272	450	20	58		3.64	790	77.5	
630	362	251	450	-20		62	3.64	882	77.0	

Table 6 (continued)

Photo Number	Run Number	T_o	P_o	α	Shock Angle Θ Windward	Shock Angle Θ Leeward	M	Re_d	Altitude	$d\Theta/\Theta$
625	357	268 °K	450 mtorr	10°	59		3.64	806	77.5	
629	361	254	450	-10		62	3.64	868	77.0	
626	358	265	450	5	59		3.64	819	77.5	
628	360	257	450	-5		63	3.64	854	77.0	
627	359	260	450	0	65		3.64	840	77.0	.49
631	363	292	1000	-20		60	3.71	1532	73.0	
633	365	292	1000	+20	50		3.71	1532	73.0	
632	364	292	1000	0	48		3.71	1532	73.0	.11
634*	404	281	100	20	51		3.20	21	97	
635*	405	281	100	10	61		3.20	21	97	
636*	406	281	100	5	57		3.20	21	97	.21
637*	407	281	100	5	61		3.20	21	97	.30
869*	423	279	1000	5	58		3.71	163	87	.27
870*	424	266	150	5	68		3.49	31	96	.49
871*	425	275	450	5	63		3.60	31	77.5	
872*	426	907	400	5	61		3.60	5	85	
873*	427	893	150	5	62		3.40	2	85.5	
874*	460	867	400	0	59		3.60	6	85	.36

*1/10 Scale Model

Table 7

Spectrographically Measured Temperatures and Densities from AEDC Tests

Run Number	Mach Number	Degrees α	Altitude km	T_R/T_s	ρ/ρ_s	x/D
26	3.71	0	72.5	1.09	1.39	.629
27	3.71	0	72.0	1.15	1.48	.011
28	3.71	0	72.0	1.07	1.39	.032
29	3.71	0	72.0	1.08	1.27	.067
30	3.71	10	72.0	1.12	.71	.043
31	3.71	10	72.0	.96	.96	.064
32	3.71	10	72.0	.85	1.20	.099
33	3.71	10	72.0	.85	1.19	.682
34	3.71	10	74.0	.77	1.57	.682
35	3.71	10	73.5	.92	1.48	.682
36	3.71	10	73.5	1.05	.78	.064
37	3.71	0	73.0	1.00	Ref	.629
39	3.71	0	73.0	.99	-	.629
40	3.71	0	73.0	1.00	1.23	.629
42	3.71	10	73.0	.87	1.28	.783
45	3.71	10	73.0	1.04	1.68	.021
46	3.71	10	73.0	1.12	1.46	.054
47	3.71	10	73.0	.94	1.36	.088
48	3.71	20	73.0	1.07	1.36	.896
50	3.71	-20	73.0	1.09	1.31	.880
51	3.71	-20	73.0	1.13	1.22	.021
54	3.71	-20	73.0	.96	1.29	.021
55	3.71	-20	73.0	1.00	1.33	.054
56	3.45	0	88.5	.92	.88	.729
57	3.45	0	89.0	.99	1.05	.032
58	3.45	0	89.0	.93	.90	.112
59	3.45	0	89.5	.85	.92	.167
60	3.45	0	89.5	.99	1.08	.086
61	3.45	0	89.5	.88	Ref	.783
62	3.45	0	89.5	.86	1.05	.783
63	3.45	0	89.5	.81	1.10	.279
64	3.45	10	89.5	1.12	1.58	0.0
65	3.45	10	89.5	1.02	1.38	.021
66	3.45	10	89.5	.86	1.06	.118
67	3.45	10	89.5	.84	1.11	.226
68	3.45	10	89.5	.83	1.13	.783

Table 7 (continued)

Run Number	Mach Number	Degrees α	Altitude km	T_R/T_s	ρ/ρ_s	x/D
69	3.45	20	89.5	1.17	1.71	0.00
70	3.45	20	89.5	1.05	1.38	.021
71	3.45	20	89.5	.87	1.12	.112
72	3.45	20	89.5	.83	1.07	.226
73	3.45	20	89.5	.83	1.10	.896
74	3.45	5	89.5	1.14	1.82	0.00
75	3.45	5	89.5	1.02	1.39	.021
76	3.45	5	89.5	.86	1.17	.112
77	3.45	5	89.5	.81	1.19	.226
78	3.45	5	89.5	.88	1.19	.757
79	3.45	-10	89.5	1.00	1.67	0.0
80	3.45	-10	89.5	1.00	1.41	.021
81	3.45	-10	89.5	.86	1.12	.112
82	3.45	-10	89.5	.87	1.09	.226
83	3.45	-10	89.5	.86	1.07	.751
111	3.6	0	84.5	1.01	Ref	.729
112	3.6	0	84.5	.91	1.40	0.00
113	3.6	0	84.5	1.04	1.16	.021
115	3.49	0	84.0	1.05	.92	.729
116	3.49	0	84.0	1.58	1.39	0.0
117	3.49	0	84.0	1.14	1.17	.011
118	3.49	0	84.0	1.01	Short	.032
119	3.49	0	84.0	1.12	.95	.032
120	3.49	0	84.0	1.09	.93	.112
121	3.49	0	84.0	1.09	.97	.220
122	3.49	0	84.0	1.06	Ref	.729
123	3.49	5	84.0	1.02	.98	.757
124	3.49	5	84.0	1.69	1.58	0.0
125	3.49	5	84.0	1.43	1.16	.021
126	3.49	5	84.0	1.22	1.19	.021
127	3.49	5	84.0	1.13	.96	.053
128	3.49	5	84.0	1.08	1.01	.112
129	3.49	5	83.5	1.07	.97	.220
130	3.49	10	83.5	1.11	1.01	.059
131	3.49	10	83.5	1.42	1.19	0.0
132	3.49	10	83.5	1.21	1.04	.021
133	3.49	10	83.5	1.04	.98	.112
134	3.49	10	83.5	1.07	.99	.220
135	3.49	10	84.0	1.05	1.02	.783
136	3.49	20	84.0	1.10	1.01	.896
137	3.49	20	84.0	1.32	1.22	0.0
138	3.49	20	84.0	1.19	1.11	.021

Table 7 (continued)

Run Number	Mach Number	Degrees α	Altitude km	T_R/T_s	ρ/ρ_s	x/D
139	3.49	20	83.5	1.10	.94	.053
140	3.49	20	83.5	1.08	.89	.112
141	3.49	20	83.5	1.06	.93	.220
142	3.49	20	83.5	1.04	.98	.020
143	3.49	20	83.5	1.09	.96	.052
144	3.49	20	84.0	1.06	1.01	.104
145	3.49	20	84.5	1.01	1.07	.730
146	3.49	-10	84.5	1.29	1.16	0.0
147	3.49	-10	84.5	1.08	.95	.021
148	3.49	-10	84.5	1.03	.91	.059
149	3.49	-10	84.5	1.04	.92	.112
150	3.49	-10	84.0	1.00	.87	.220
151	3.49	-10	84.0	1.06	.89	.751
175	3.64	0	77.5	1.07	1.12	0.0
176	3.64	0	77.5	1.09	.98	.021
177	3.64	0	77.5	1.05	.95	.053
178	3.64	0	77.5	1.07	.84	.112
179	3.64	0	77.5	1.07	.83	.220
180	3.64	0	77.5	1.04	.91	.729
181	3.64	5	77.5	1.20	1.04	0.0
182	3.64	5	77.5	1.06	.91	.021
183	3.64	5	77.5	1.00	1.01	.053
184	3.64	5	77.5	1.09	.93	.112
185	3.64	5	77.5	1.03	.89	220
186	3.64	5	77.5	1.02	Ref	.757
187	3.64	10	77.5	1.01	.93	.783
188	3.64	10	77.5	1.11	.99	0.0
189	3.64	10	77.5	1.07	.92	.021
190	3.64	10	77.5	1.04	.97	.053
232	3.20	0	84.0	1.01	1.02	.729
233	3.20	0	84.0	1.01	Ref	.729
234	3.20	0	84.0	1.02	.98	.220
235	3.20	0	84.0	1.14	1.09	0.0
236	3.20	0	84.0	1.14	1.08	0.0
237	3.20	0	84.0	1.07	.99	.021
238	3.20	0	84.0	1.04	.97	.053
239	3.20	0	84.0	1.02	.98	.112
240	3.20	10	84.0	1.04	.97	.783
241	3.20	10	84.0	1.22	1.13	0.0
242	3.20	10	84.0	1.07	1.01	.021
243	3.20	10	84.0	1.05	.97	.053
244	3.20	10	84.0	1.01	.97	.123
245	3.20	10	84.0	1.02	.96	.220

Table 7 (continued)

Run Number	Mach Number	Degrees α	Altitude km	T_R/T_s	ρ/ρ_s	x/D
246	3.20	20	84.0	1.02	1.00	.896
247	3.20	20	84.0	1.08	1.07	0.0
248	3.20	20	84.0	1.06	1.02	.021
249	3.20	20	84.0	1.06	1.01	.053
250	3.20	20	84.0	1.04	.98	.123
251	3.20	20	84.0	1.02	.99	220
273	3.16	20	90.0	.93	Ref	.896
274	3.16	20	90.0	1.01	1.27	0.0
275	3.16	20	90.0	1.08	1.17	.021
276	3.16	20	90.0	1.00	1.05	.053
277	3.16	20	90.0	.97	.95	.112
278	3.16	20	90.0	.91	.97	.220
279	3.16	10	90.0	.96	.95	.783
280	3.16	10	90.0	1.03	1.18	0.0
281	3.16	10	90.0	1.07	1.01	.021
282	3.16	10	90.0	1.00	.99	.053
283	3.16	10	90.0	.92	.97	.112
284	3.16	10	90.0	.88	.98	.220
285	3.16	0	90.0	.96	.96	.729
286	3.16	0	90.0	1.11	1.05	0.0
287	3.16	0	90.0	1.00	.93	.112
288	3.16	0	90.0	.92	.92	.226
300	3.60	0	84.5	.95	.17	.729
301	3.60	0	84.5	.96	1.09	.011
302	3.60	0	84.5	1.22	.98	.032
303	3.60	0	84.5	1.01	.90	.053
304	3.60	0	84.5	.90	1.01	.112
305	3.60	0	84.5	.84	.95	.220
306	3.60	10	84.5	.90	Ref	.783
307	3.60	10	84.5	.91	1.03	.053
308	3.60	10	84.5	.92	.96	.076
309	3.60	10	84.5	.94	.96	.108
310	3.60	10	84.5	.93	.97	.167
311	3.60	10	84.5	.90	.97	.273
312	3.60	20	84.5	.93	1.03	.896
313	3.60	20	84.5	1.15	1.11	0.0
314	3.60	20	84.5	.96	1.13	.021
315	3.60	20	84.5	1.01	1.00	.053
316	3.60	20	84.5	.95	1.02	.220

Table 7 (continued)

Run Number	Mach Number	Degrees α	Altitude km	T_R/T_s	ρ/ρ_s	x/D
317	3.60	-10	84.5	.93	1.03	.751
318	3.60	-10	84.5	1.09	1.40	0.0
319	3.60	-10	84.5	.91	1.01	.112
341	3.64	20	81.5	.90	1.05	0.0
342	3.64	20	81.0	.91	1.06	.021
343	3.64	20	81.0	.88	1.02	.053
344	3.64	20	81.0	.90	1.03	.220
345	3.64	10	80.5	.92	.92	.108
346	3.64	10	80.5	.93	.99	.273
347	3.64	-10	80.0	1.00	.91	.751
348	3.64	-10	79.5	.96	1.00	.112
408*	3.20	5.5	97.0	1.24	1.15	0.0
409*	3.20	5.5	97.0	1.11	.982	.21
410*	3.20	5.5	97.0	1.10	.954	.53
411*	3.20	5.5	97.0	1.09	.916	1.34
412*	3.20	5.5	97.0	1.06	.931	2.41
413*	3.20	5.5	97.0	1.07	.998	3.49
414*	3.20	5.5	97.0	1.03	Ref	6.43
415*	3.71	5.5	87.0	1.07	1.24	0.0
416*	3.71	5.5	87.0	1.06	1.23	0.0
417*	3.71	5.5	87.0	1.00	1.14	.53
418*	3.71	5.5	87.0	1.03	1.03	.53
419*	3.71	5.5	87.0	1.06	.93	1.34
420*	3.71	5.5	87.0	1.08	.96	1.37
421*	3.71	5.5	87.0	1.05	1.01	2.41
422*	3.71	5.5	87.0	1.04	Ref	2.41
428*	3.45	5.5	103	1.06	1.73	0.0
429*	3.45	5.5	103	1.07	1.80	0.0
430*	3.45	5.5	103	1.09	1.45	.21
431*	3.45	5.5	103	.97	1.29	.53
432*	3.45	5.5	103	.88	1.21	1.34
433*	3.45	5.5	103	.82	1.16	2.41
434*	3.45	5.5	103	.93	1.08	3.49
435*	3.45	5.5	103	.94	Ref	6.01
436*	3.60	5.5	98	1.02	1.13	.11
437*	3.60	5.5	98	.98	1.13	.21
438*	3.60	5.5	98	.93	1.05	.53
439*	3.60	5.5	98	.90	.97	1.34
440*	3.60	5.5	98	.91	1.01	2.41
441*	3.60	5.5	98	.91	.97	3.49
442*	3.60	5.5	98	.91	Ref	6.01

*Runs from 408-449 were for 1/10 scale model. All others were full-scale model.

Table 7 (continued)

Run Number	Mach Number	Degrees α	Altitude km	T_R/T_s	ρ/ρ_s	x/D
443*	3.45	0	103	.97	2.67	0.0
444*	3.45	0	103	1.03	1.61	.11
445*	3.45	0	103	.89	1.58	.32
446*	3.45	0	103	.87	1.45	1.12
447*	3.45	0	103	.87	1.26	2.18
448*	3.45	0	103	.87	1.23	3.27
449*	3.45	0	103	.81	1.24	5.79

*Runs from 408-449 were for 1/10 scale model. All others were full-scale model.

Precedeing Page Blank - not Filmed

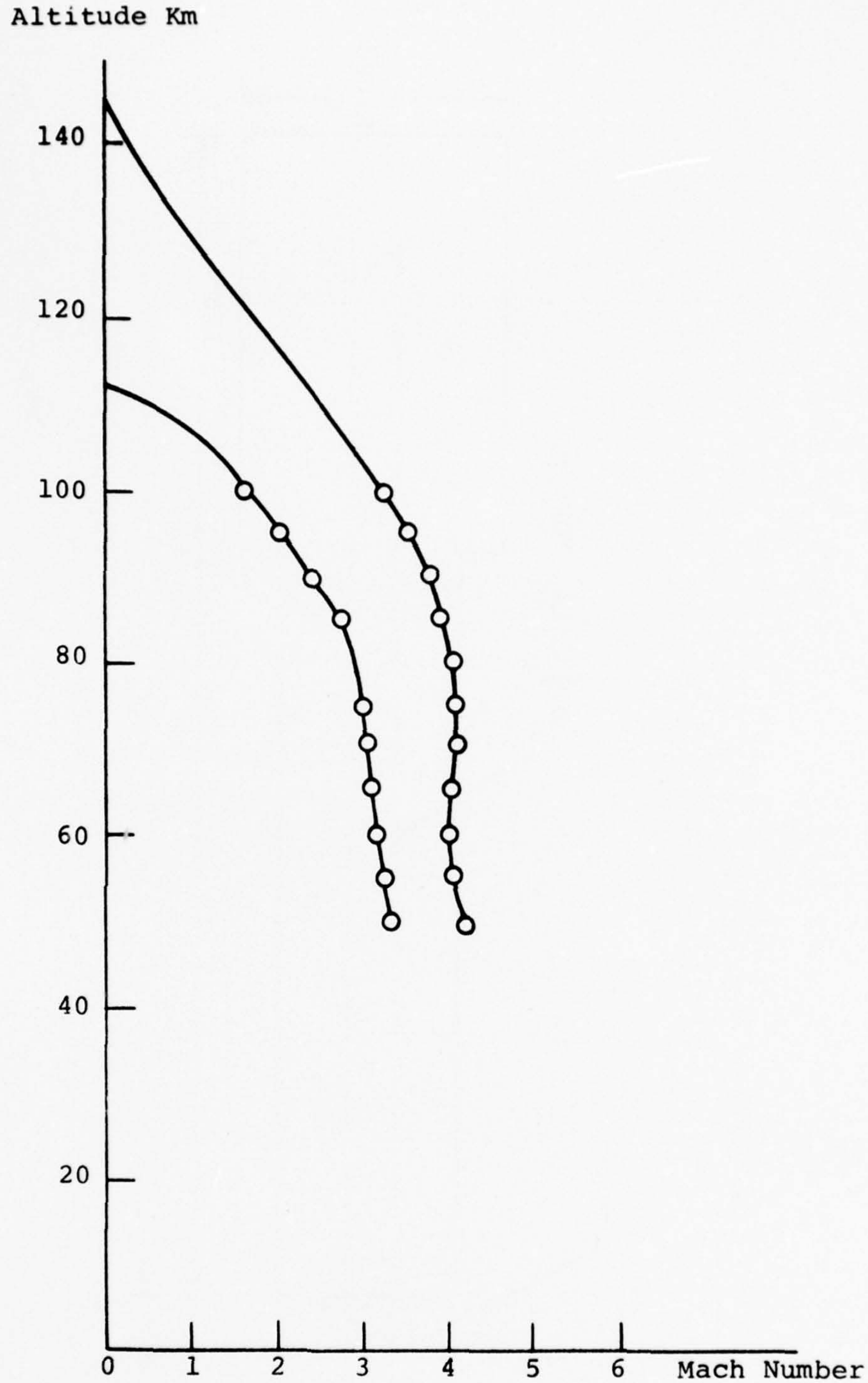

Figure 1. Limiting Flight Corridors for UTE Tomahawk

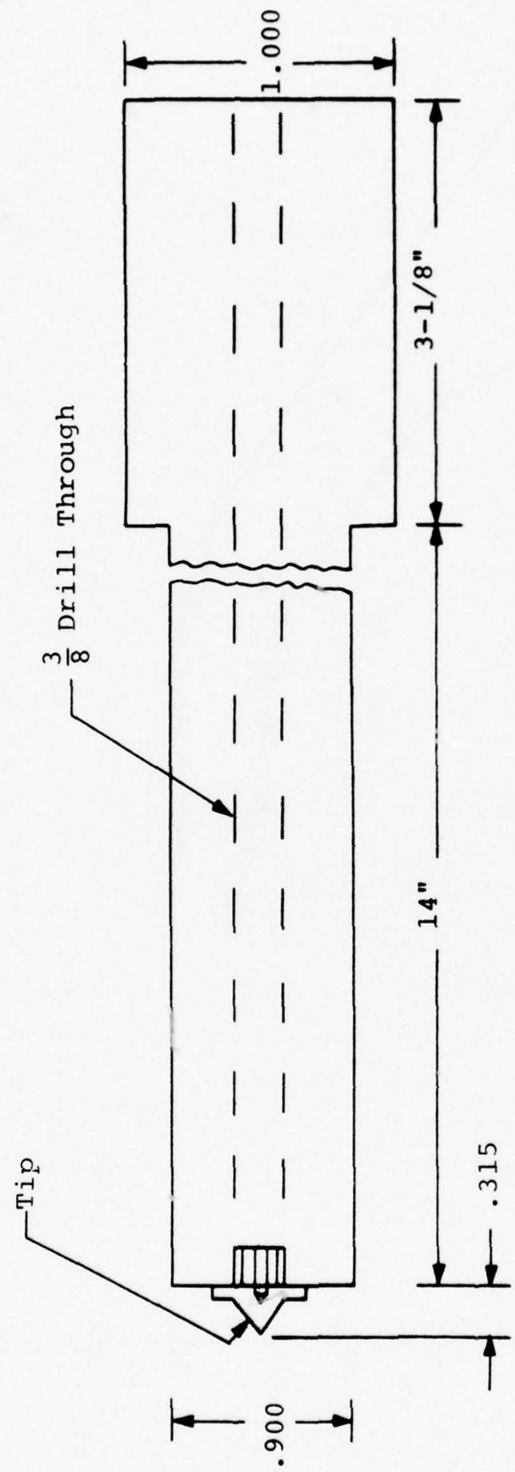

Figure 2. AFGL Blunt Skimmer Model

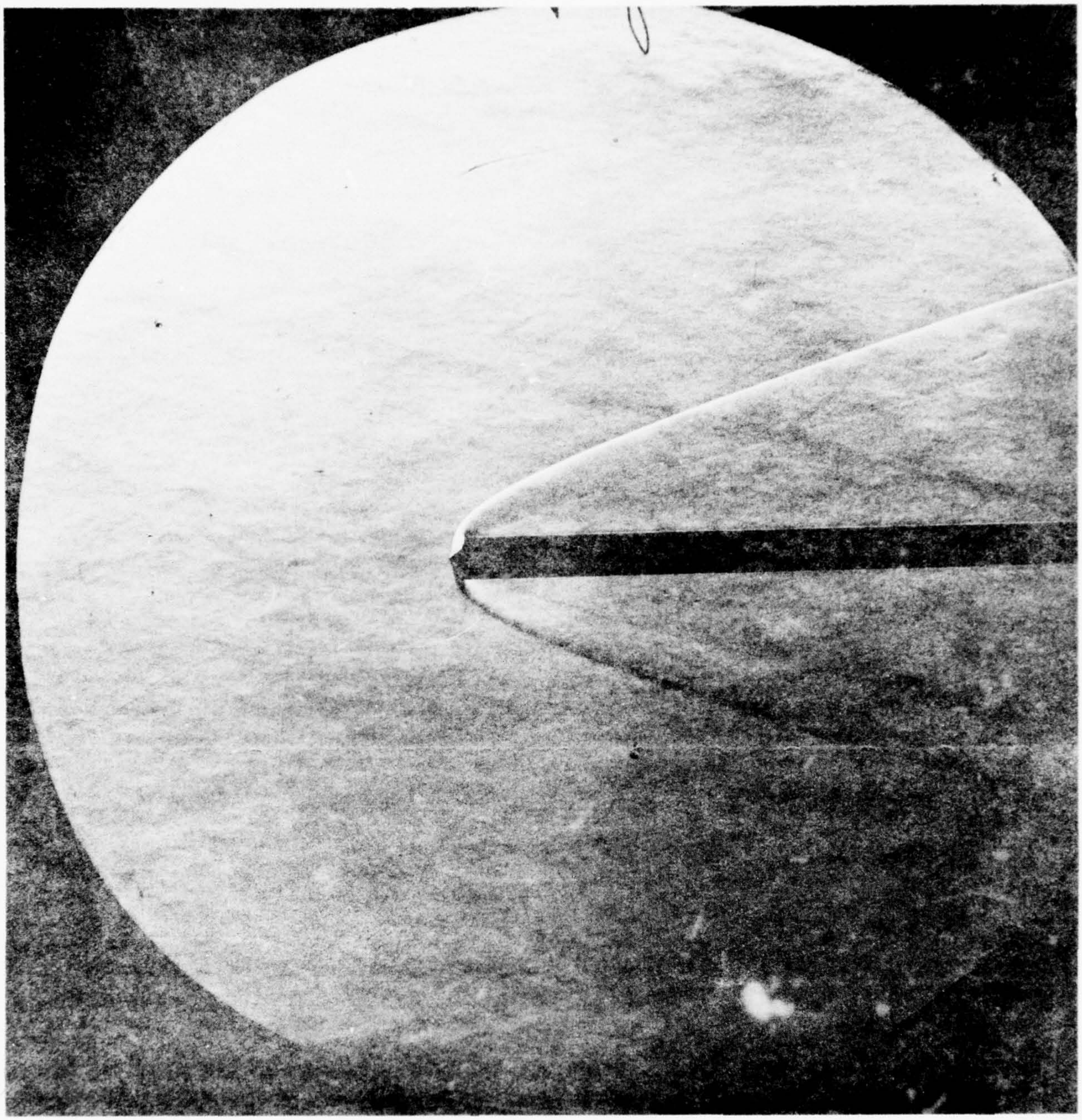

Figure 3. Blunt Model at M=4 and Equivalent Altitude of 39.5 Km
- Shock Attached

Photo 65020

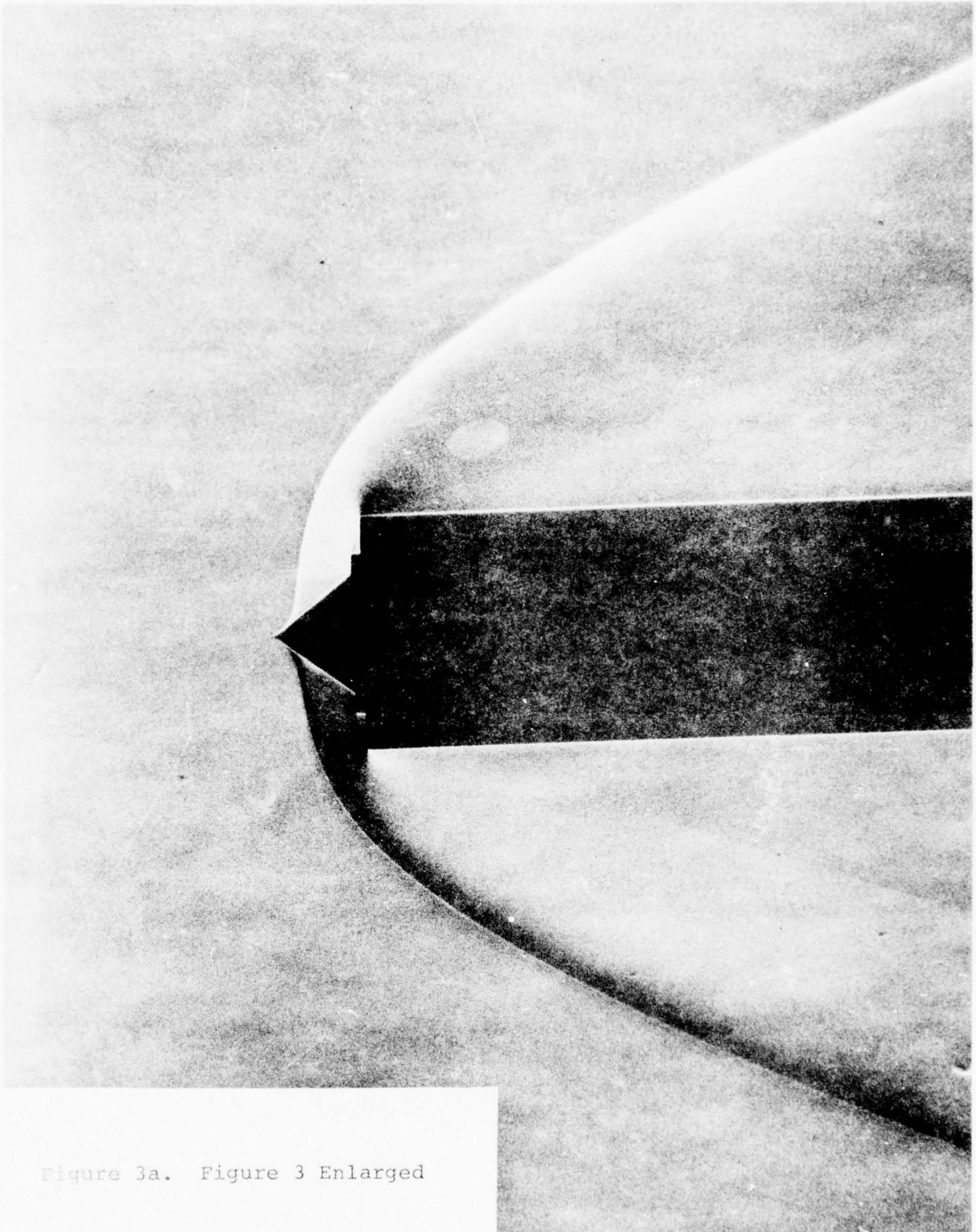

Figure 3a. Figure 3 Enlarged

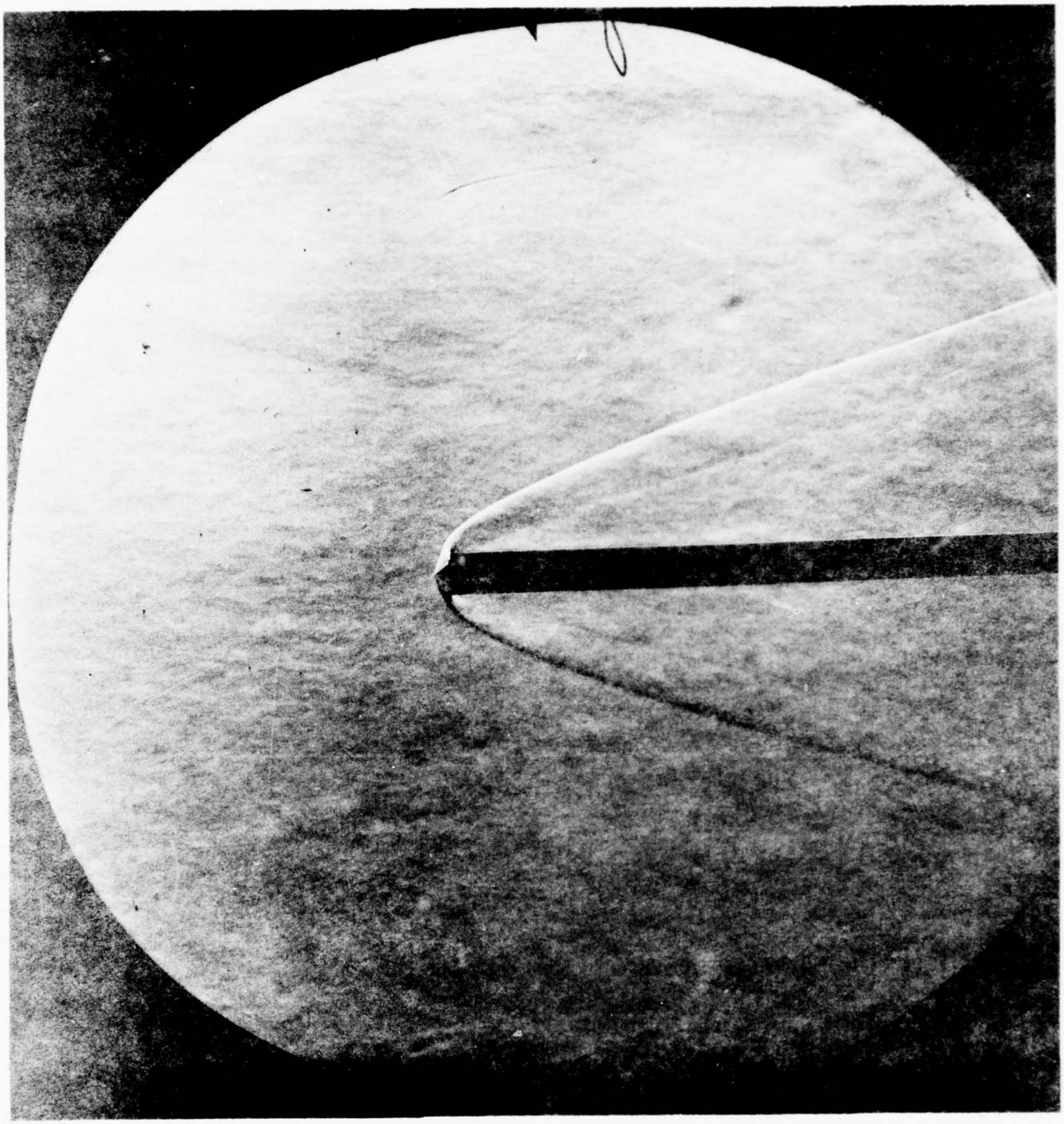

Figure 4. Alternate Shock Position on Blunt Model at M=4 and 39.5 Km Equivalent Altitude - Shock Detached

Photo 65021

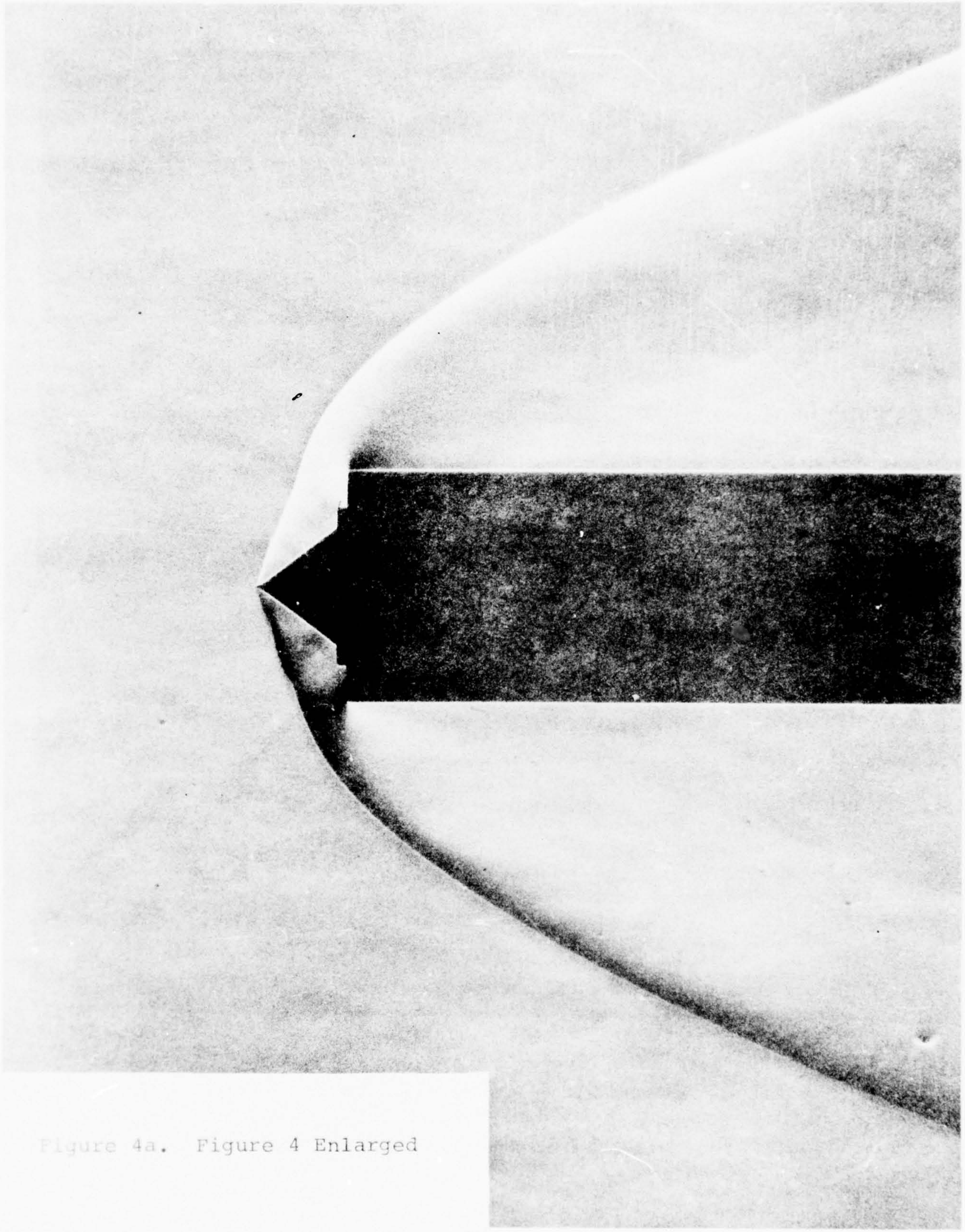

Figure 4a. Figure 4 Enlarged

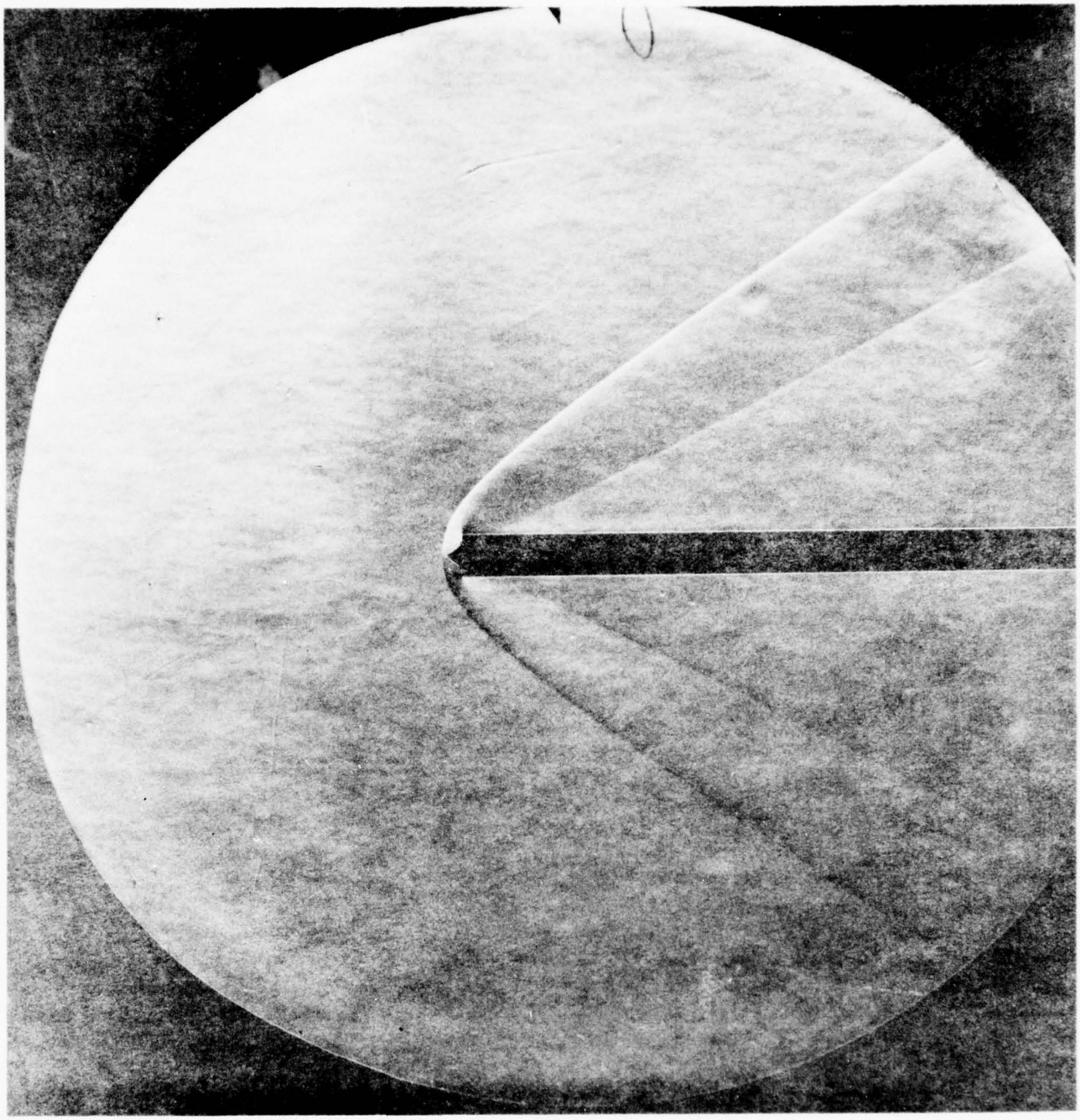

Figure 5. Blunt Model at M=2 and 38 Km Equivalent Altitude
Photo 65031

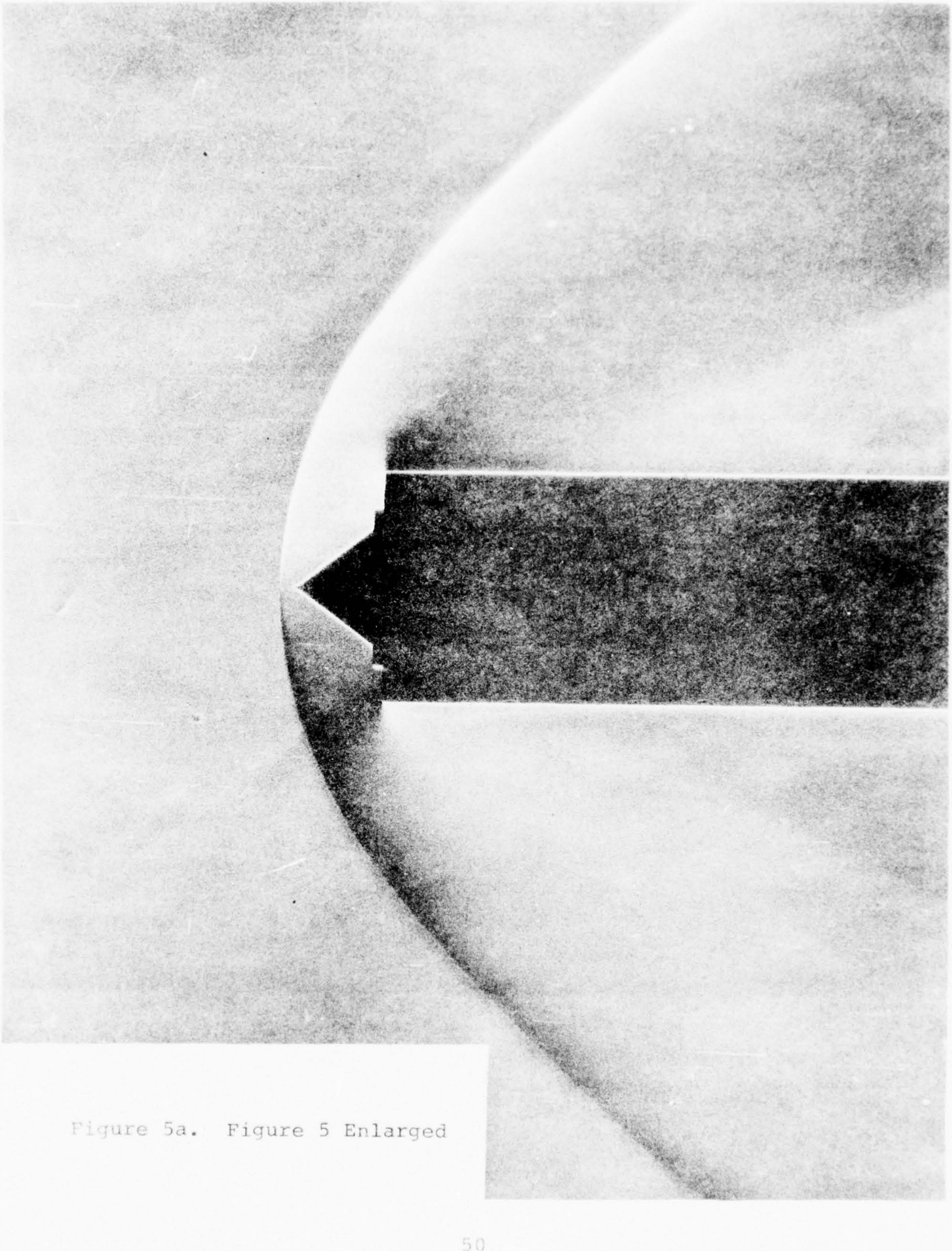

Figure 5a. Figure 5 Enlarged

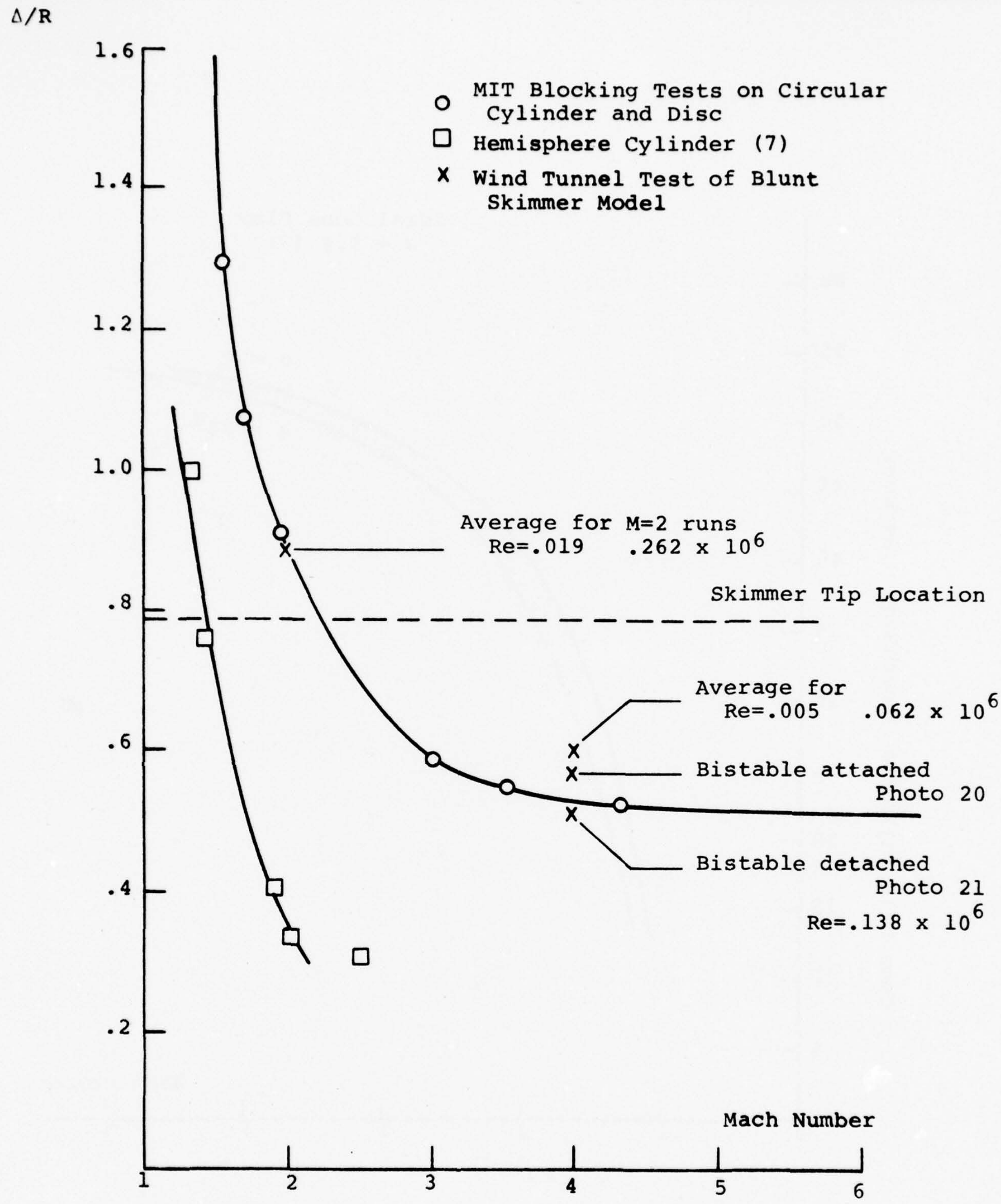

Figure 6. Shock Standoff Distance from Blunt Skimmer compared to Cylinders and Hemisphere Cylinders

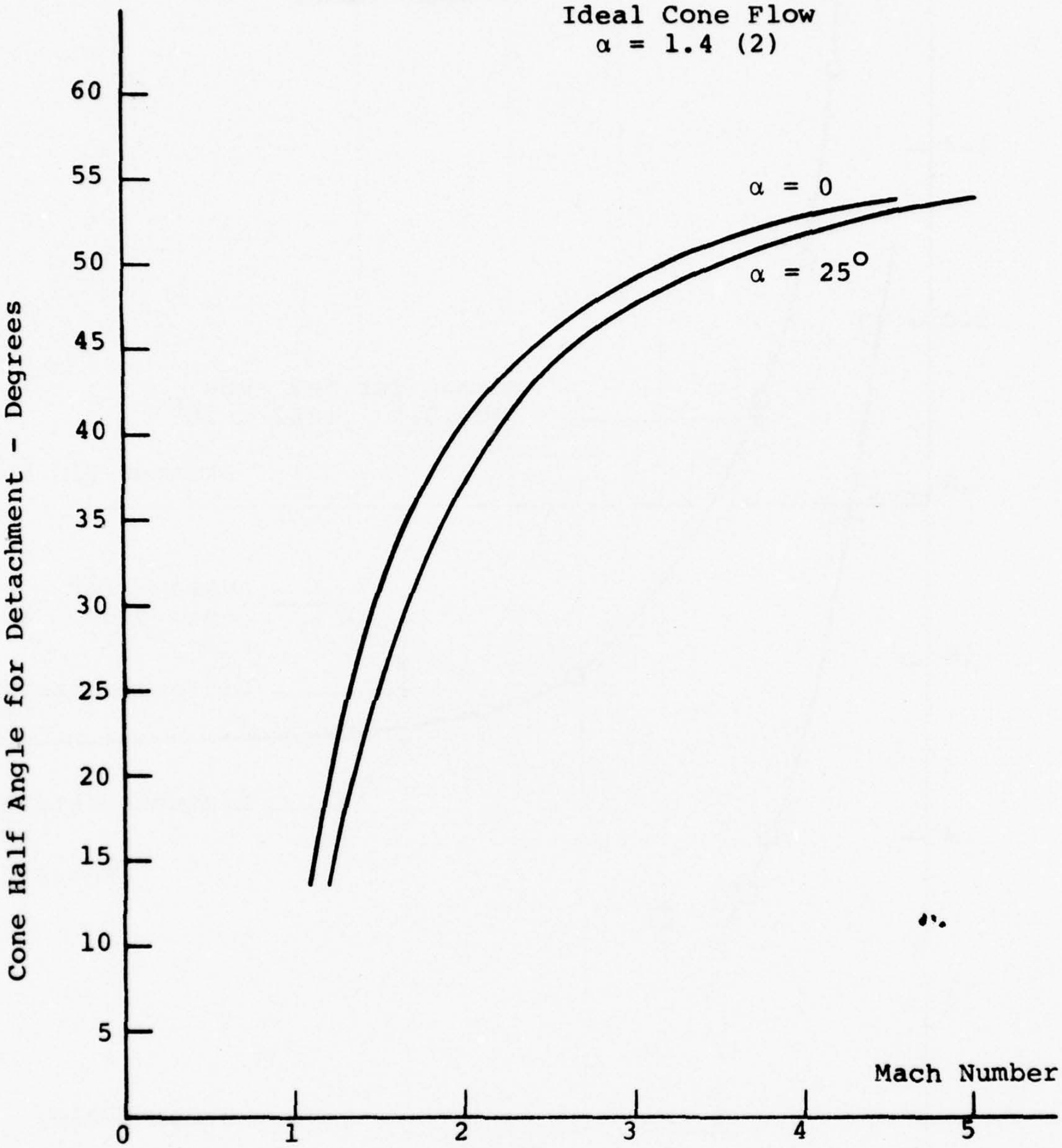

Figure 7. Cone Angle for Shock Wave Detachment vs. Mach Number

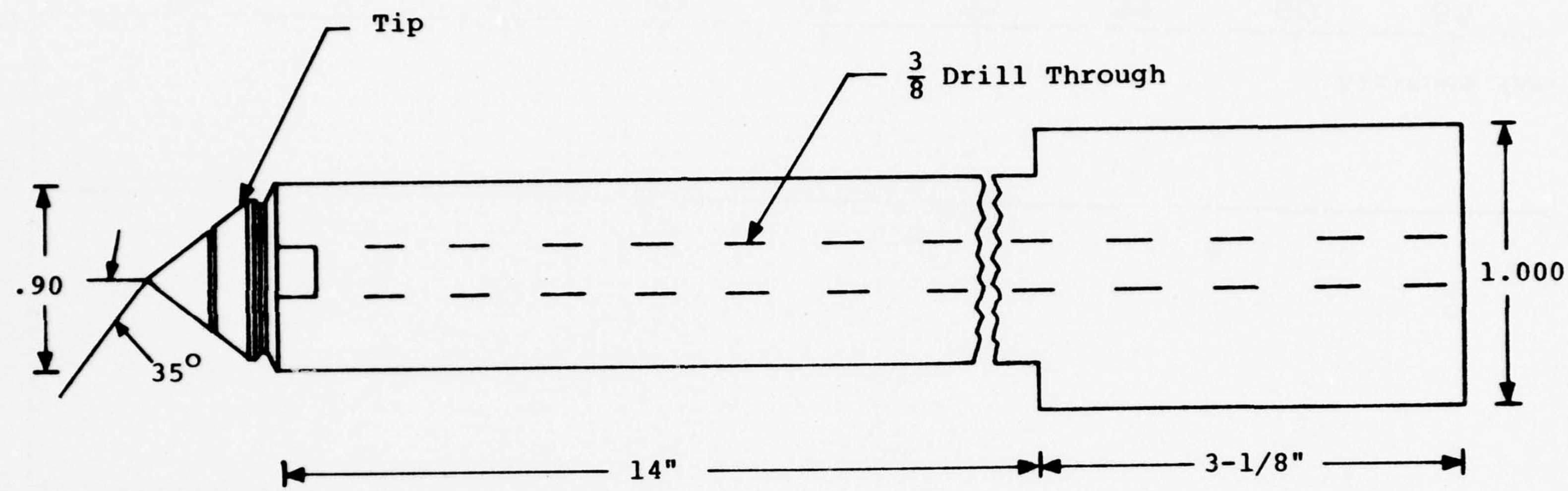

Figure 8. AFGL 35° Conical Skimmer Model

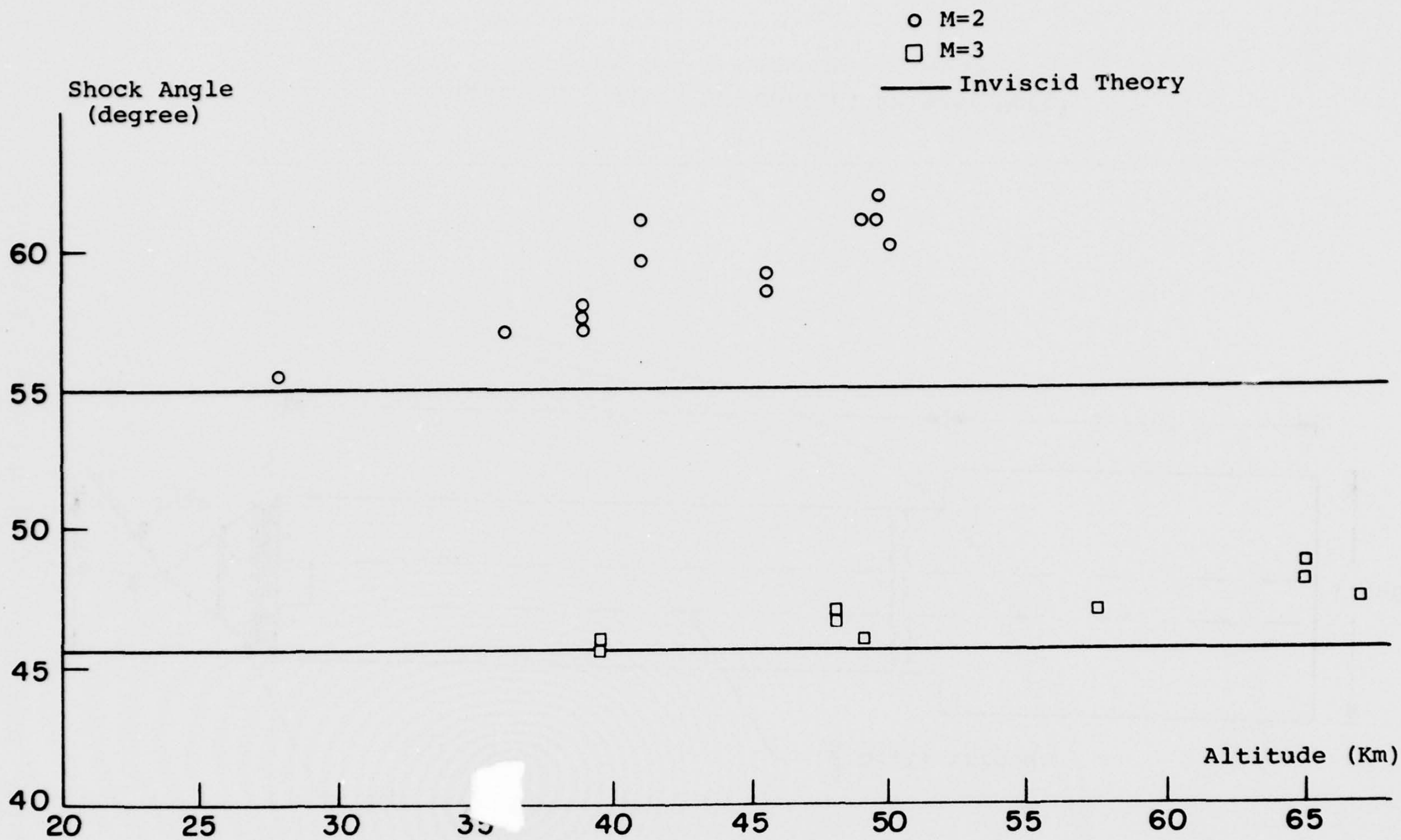

Figure 9. Shock Angle Data for 35° Conical Model vs. Altitude for Zero Angle of Attack

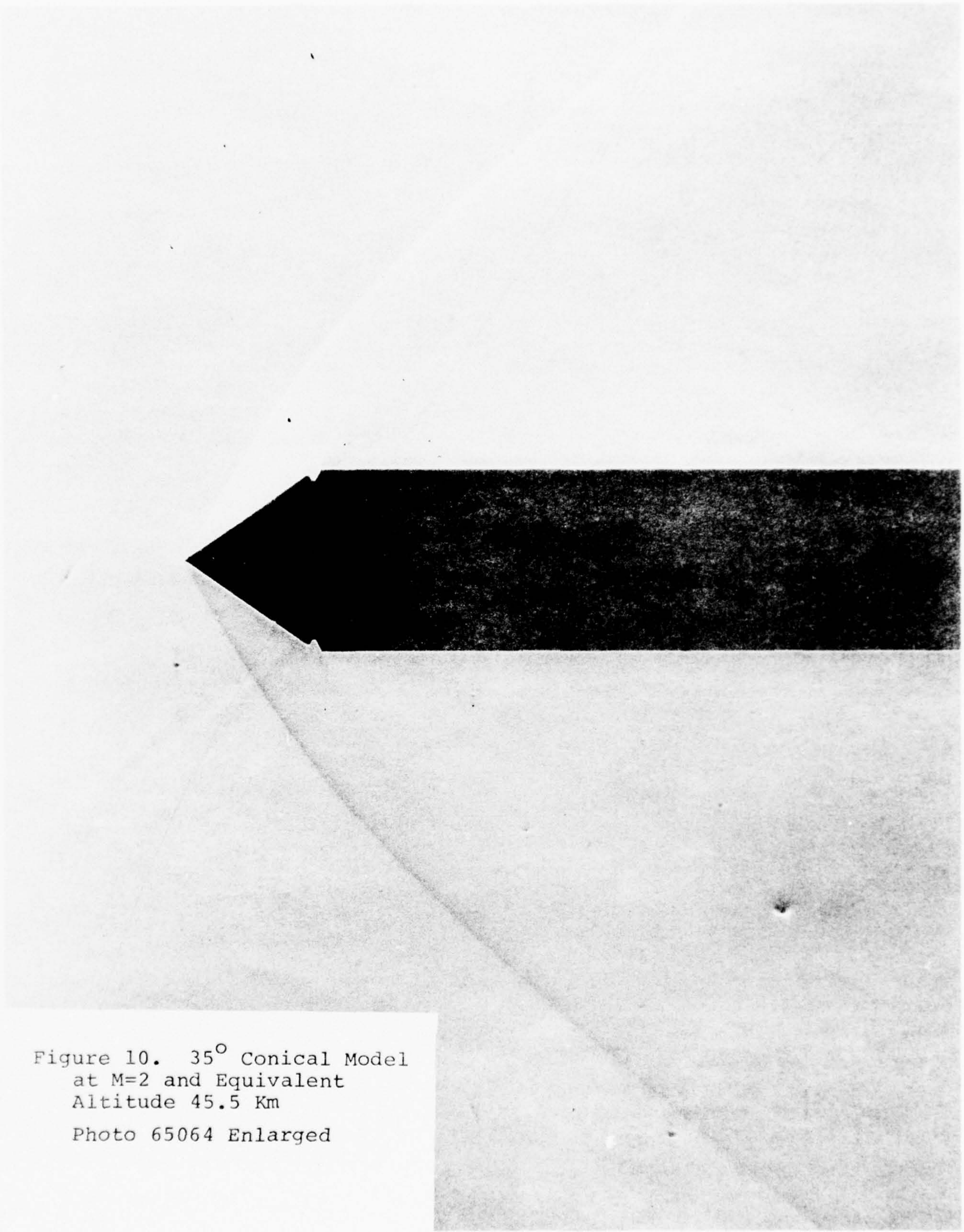

Figure 10. 35° Conical Model at M=2 and Equivalent Altitude 45.5 Km

Photo 65064 Enlarged

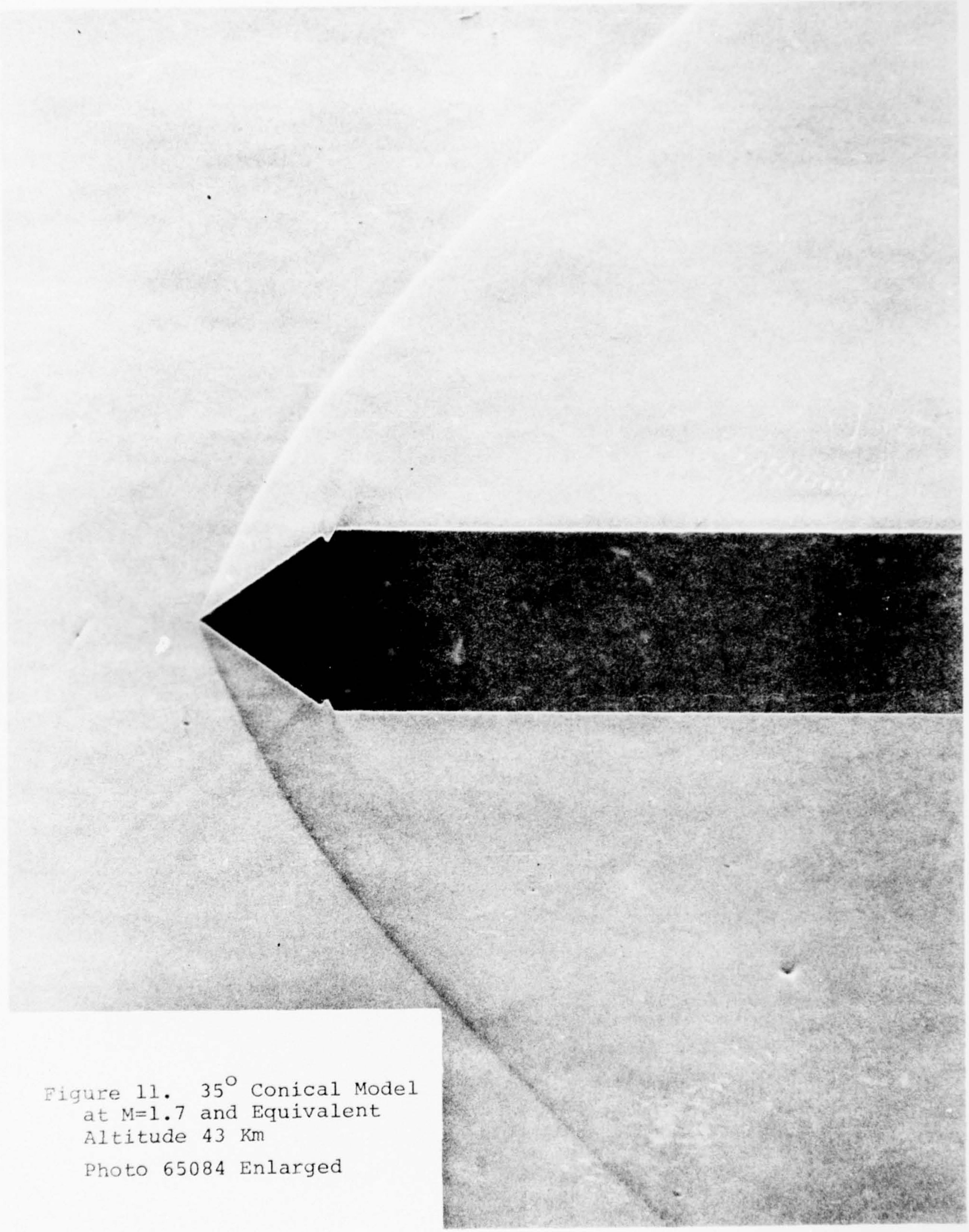

Figure 11. 35° Conical Model at M=1.7 and Equivalent Altitude 43 Km

Photo 65084 Enlarged

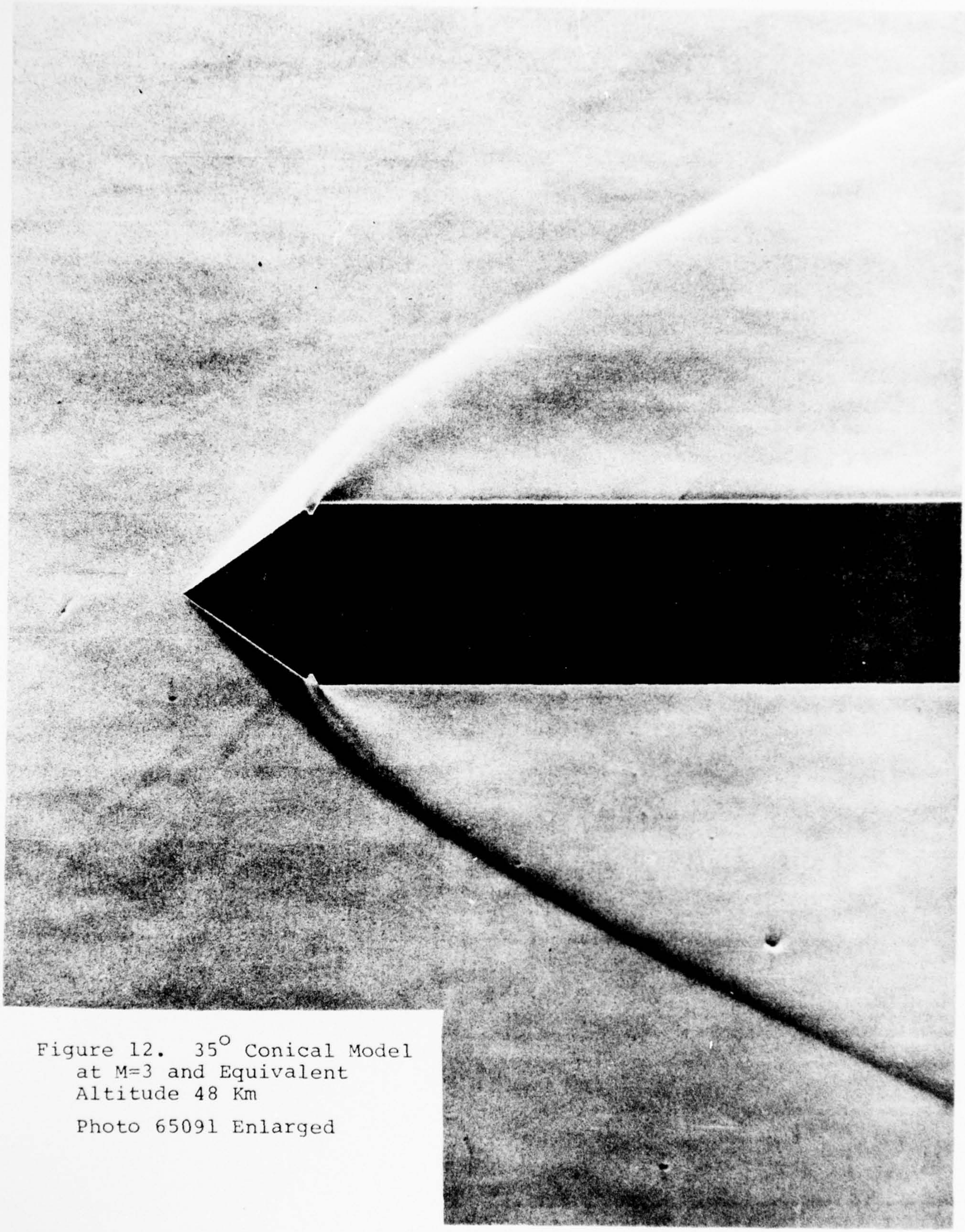

Figure 12. 35° Conical Model at M=3 and Equivalent Altitude 48 Km

Photo 65091 Enlarged

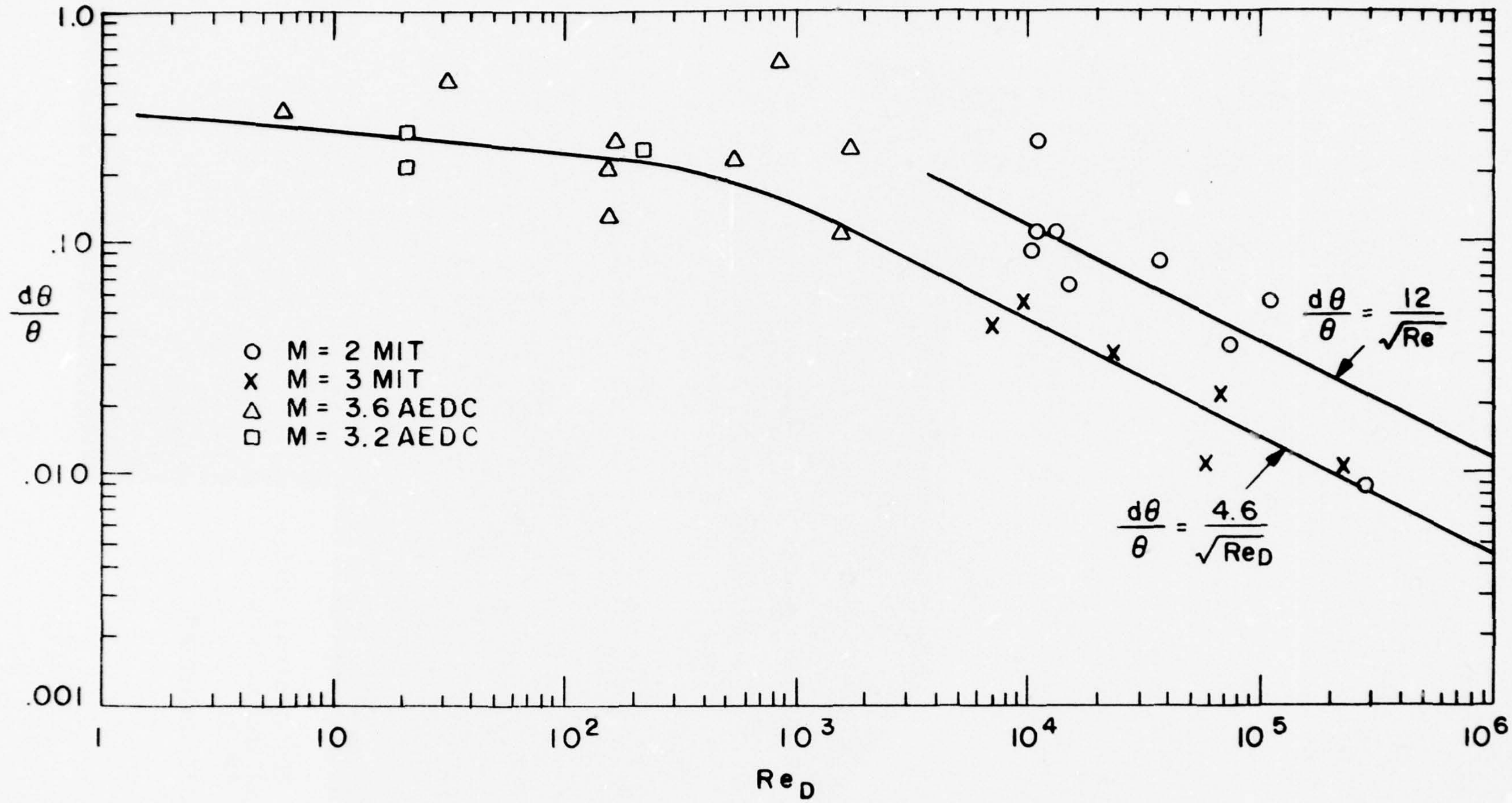

Figure 13. Change in Shock Angle vs. Reynolds Number

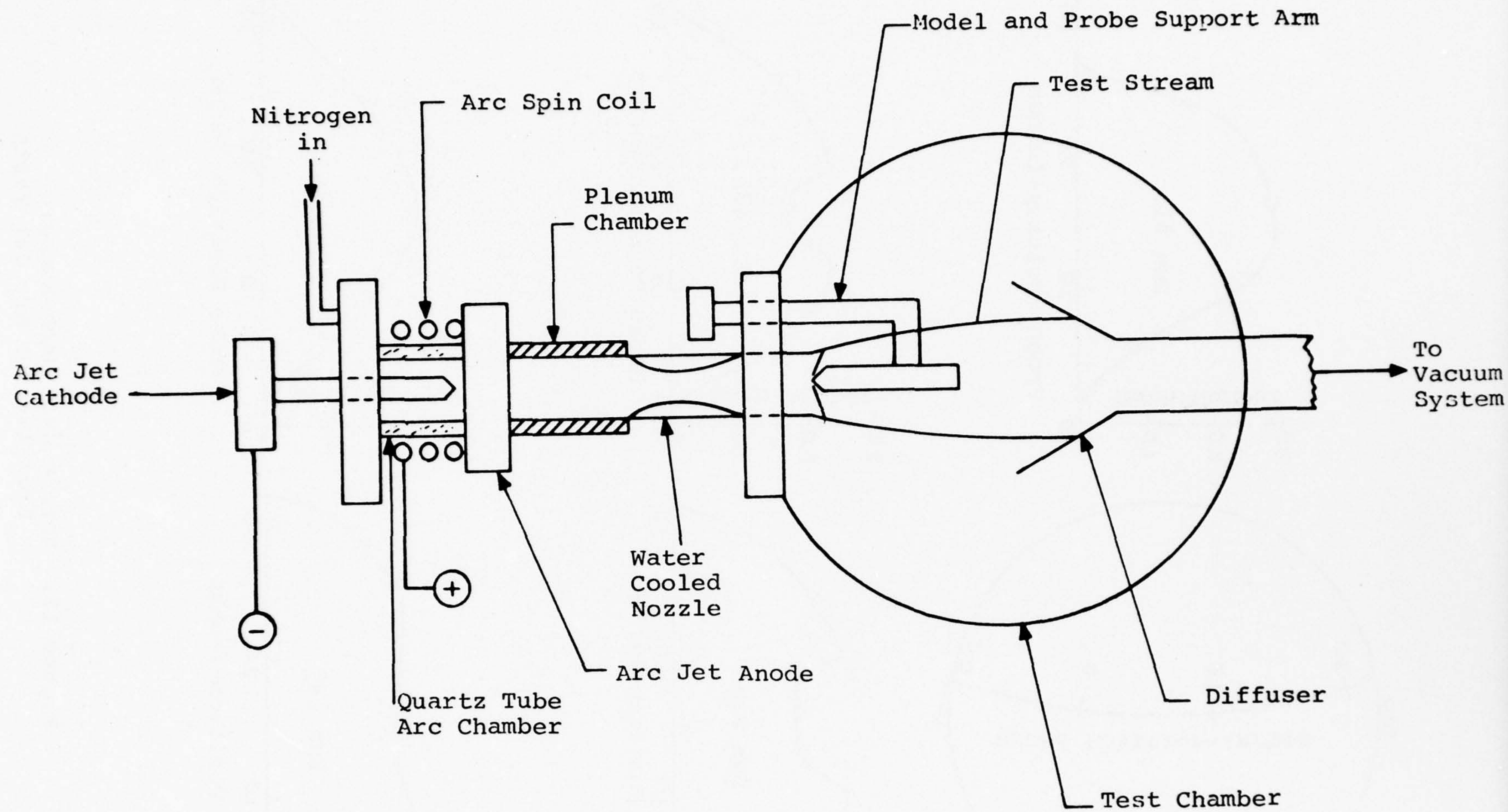

Figure 14. MIT Arc Jet Test Configuration

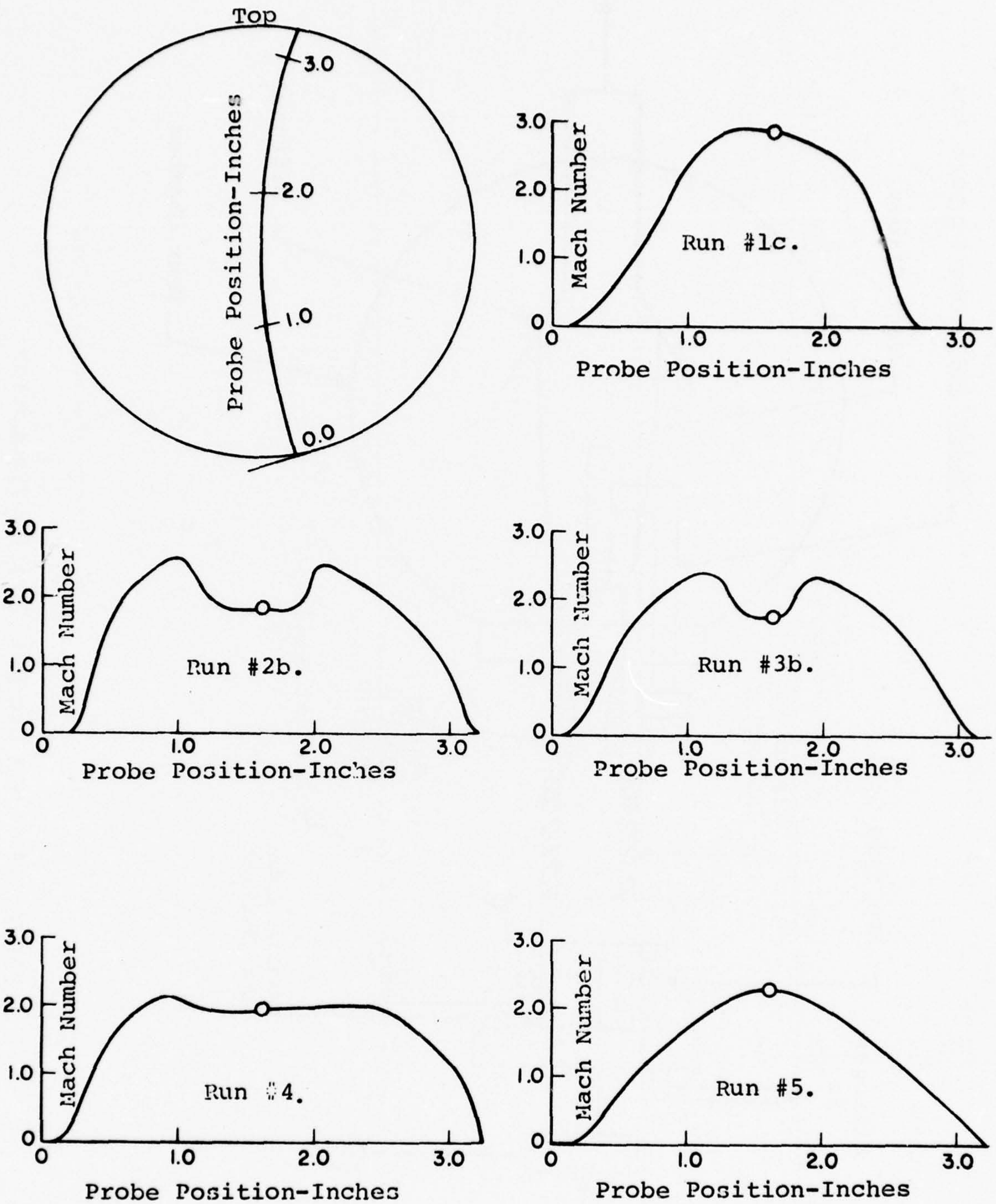

Figure 15. Nozzle Exit Mach Number Profiles for Arc Jet Tests

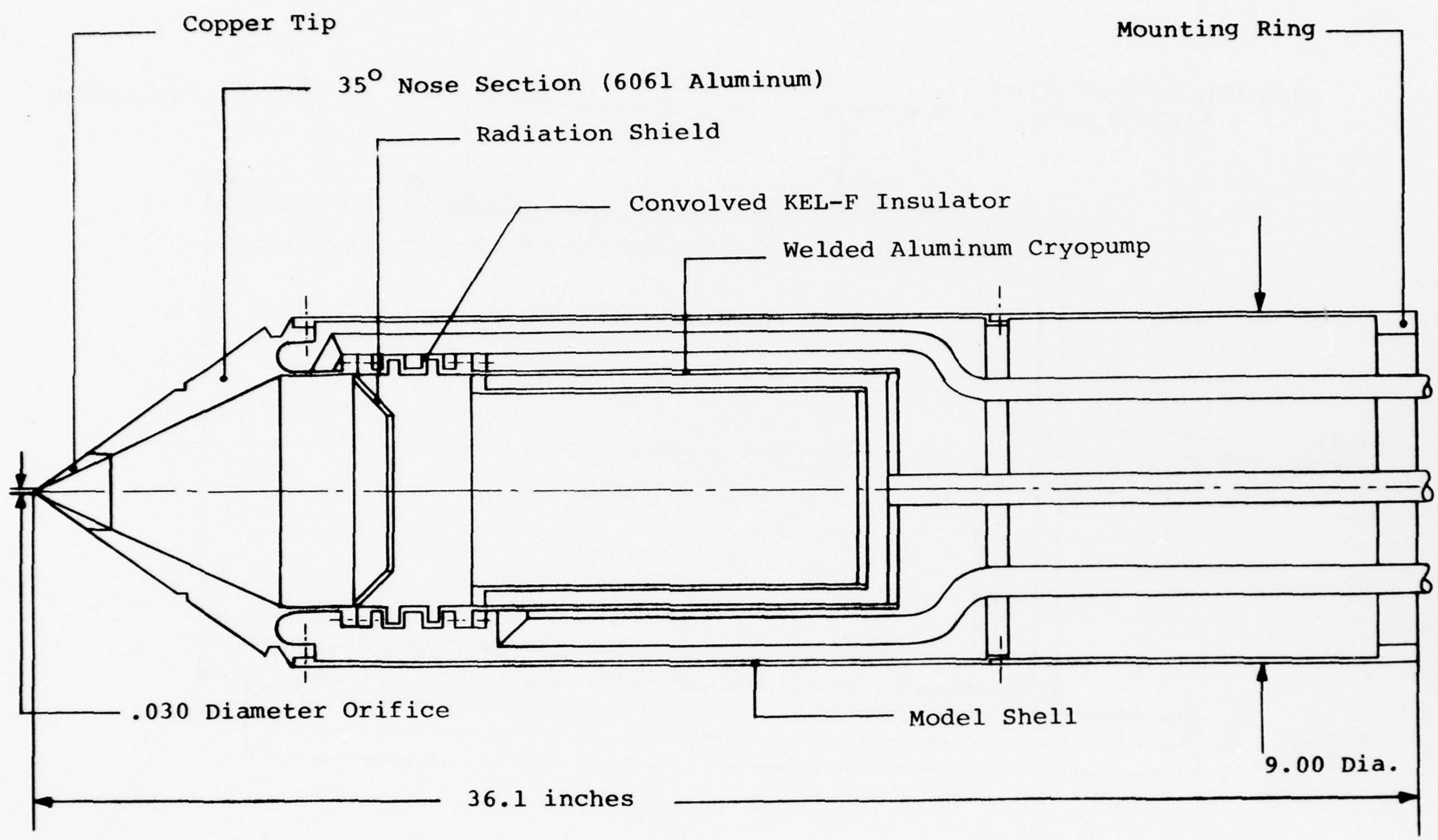

Figure 16. Full Scale Aspirated Skimmer Model Cross Section

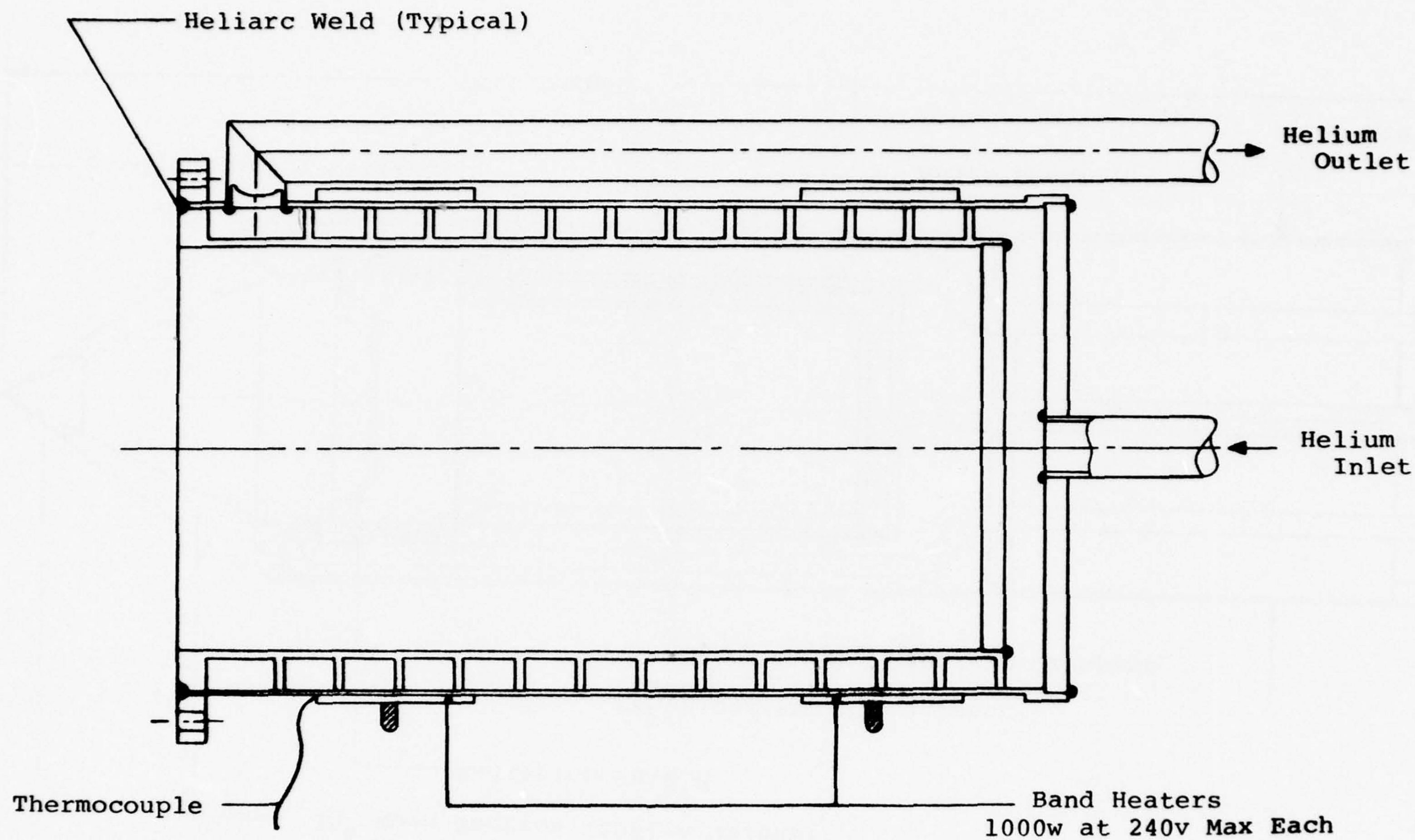

Figure 17. Cryopump Assembly Cross Section

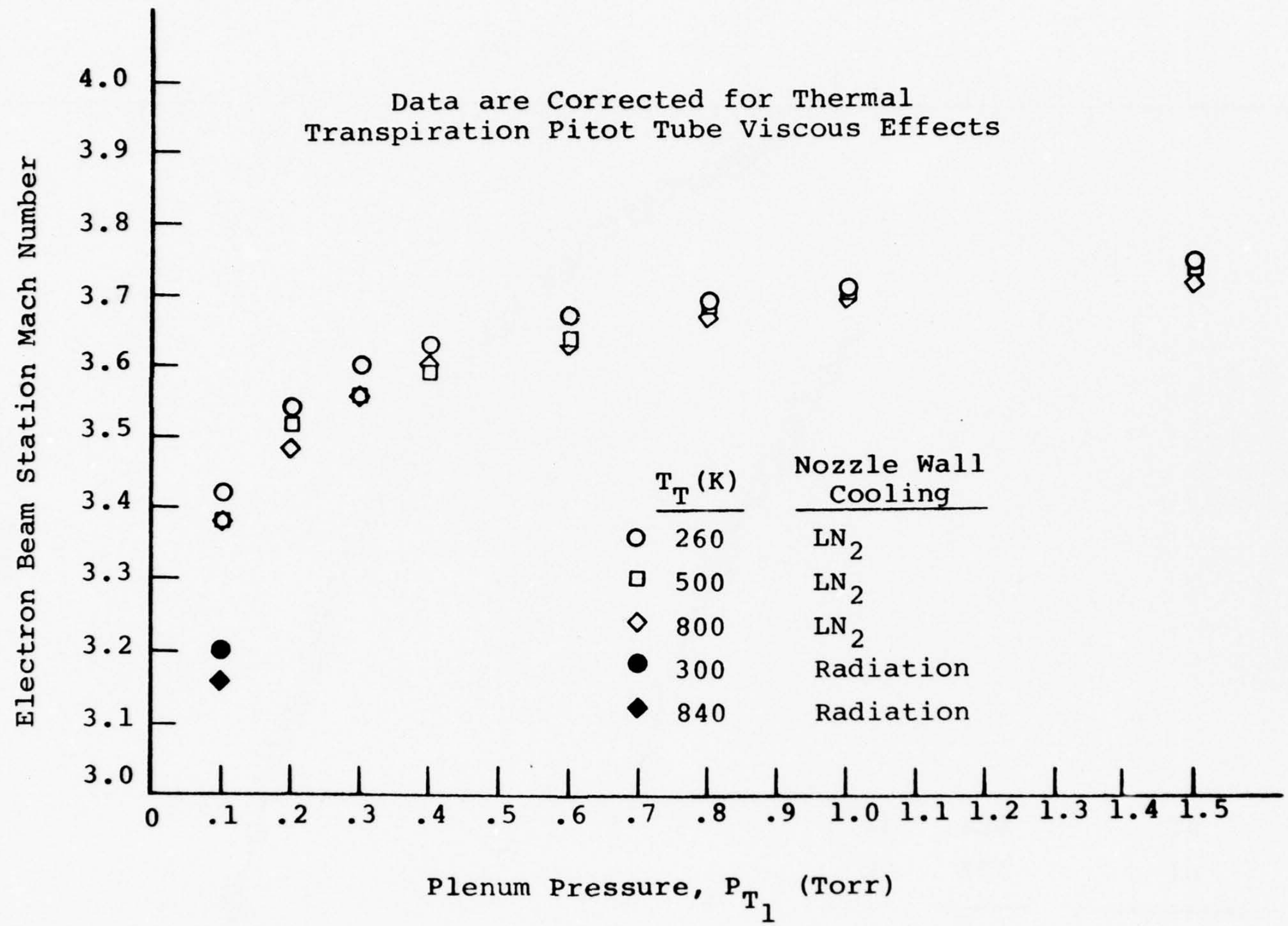

Figure 18. Mach Number at Test Station as a Function of Plenum Pressure

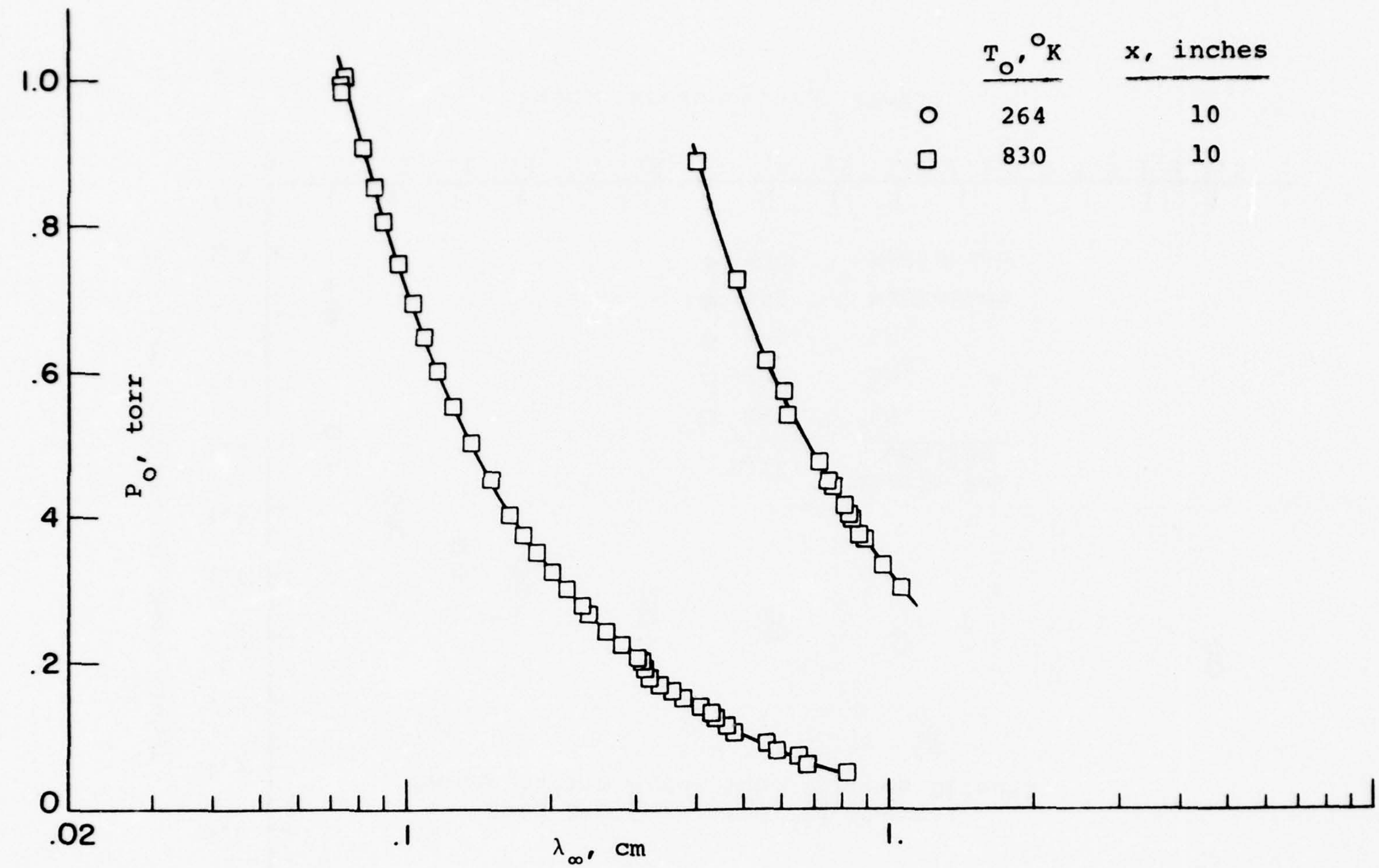

Figure 19. Mean Free Path in the Mach 3 Nozzle Test Section

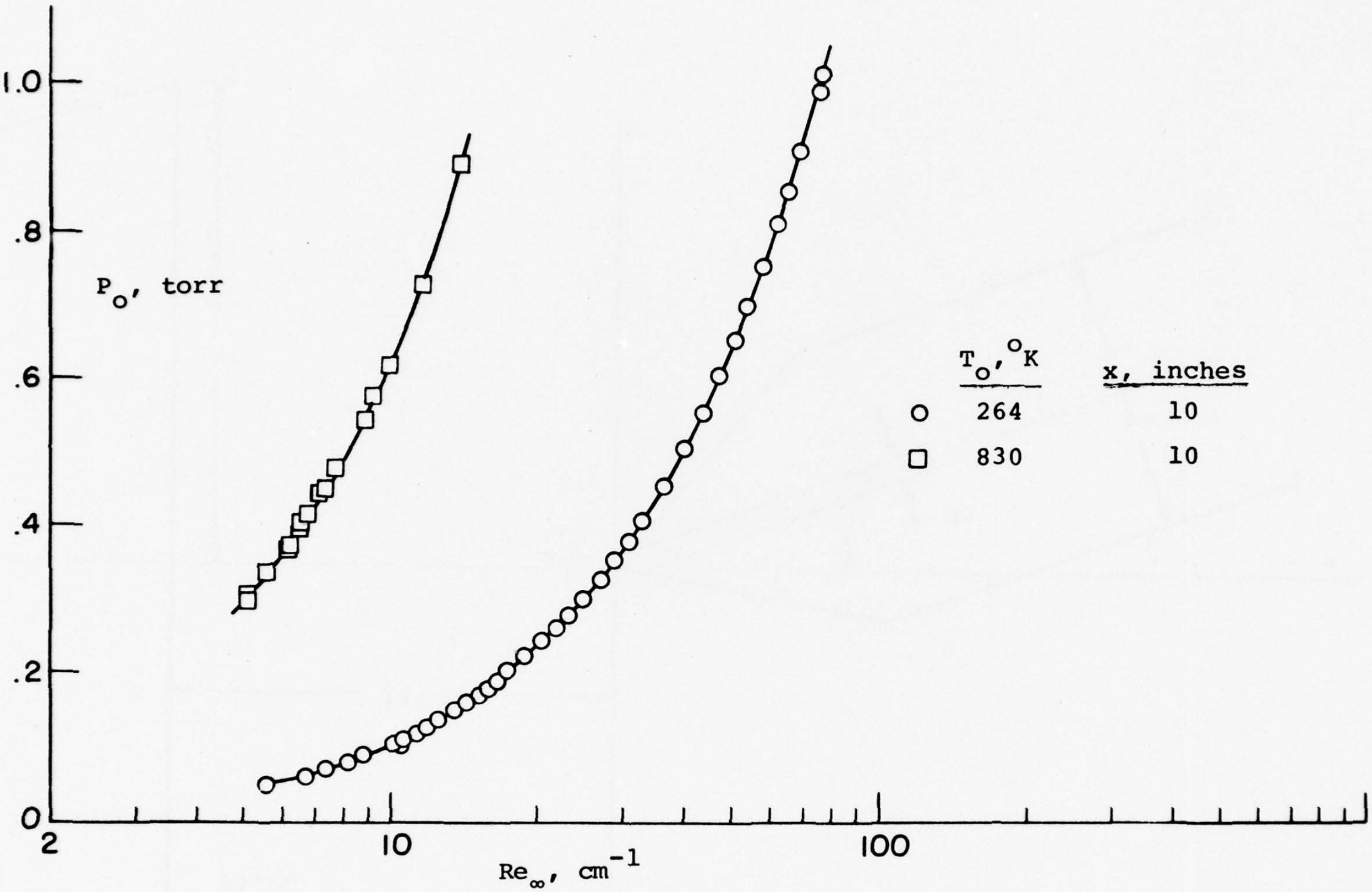

Figure 20. Unit Reynolds Number in the M3 Nozzle Test Section

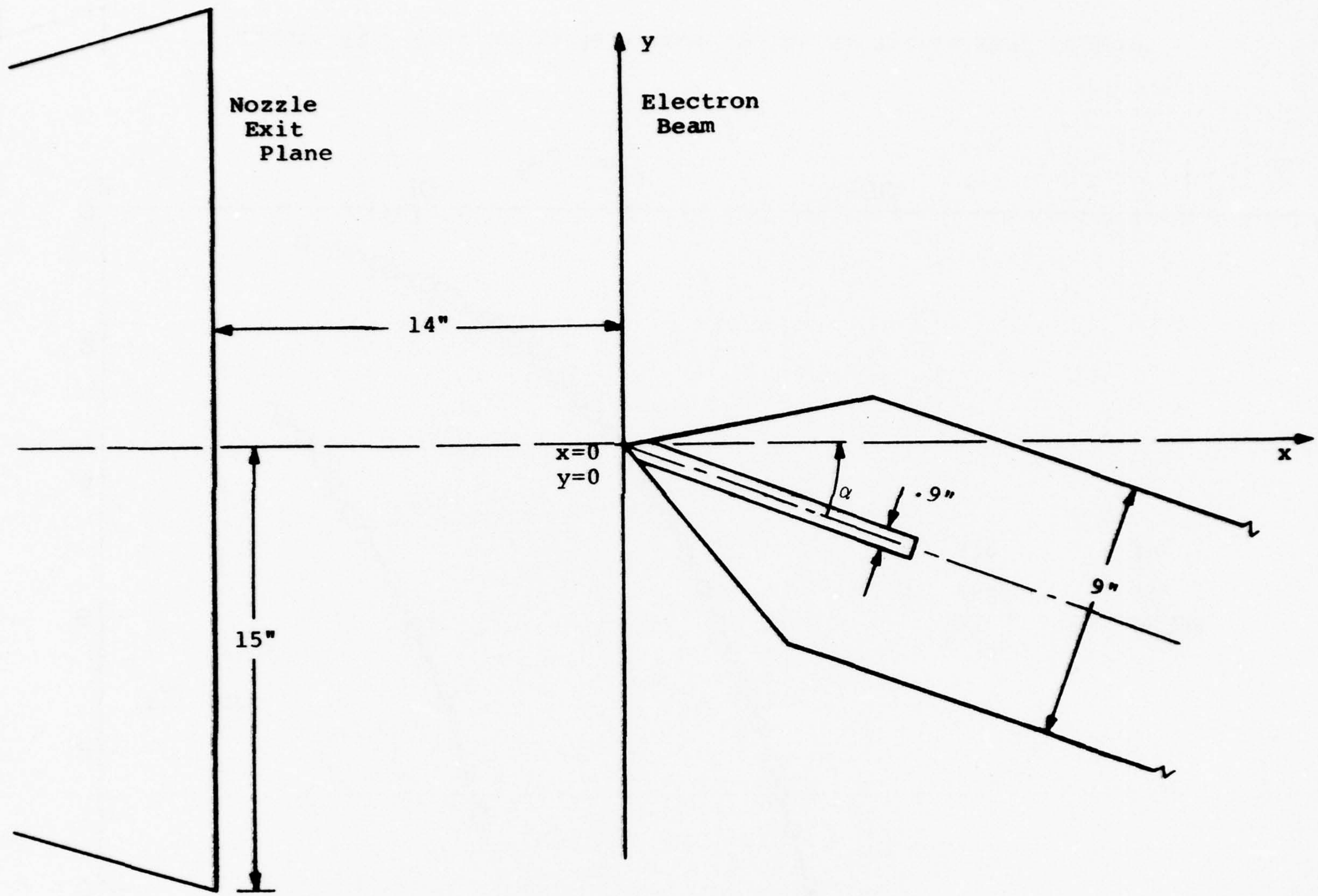

Figure 21. Schematic of Experimental Setup

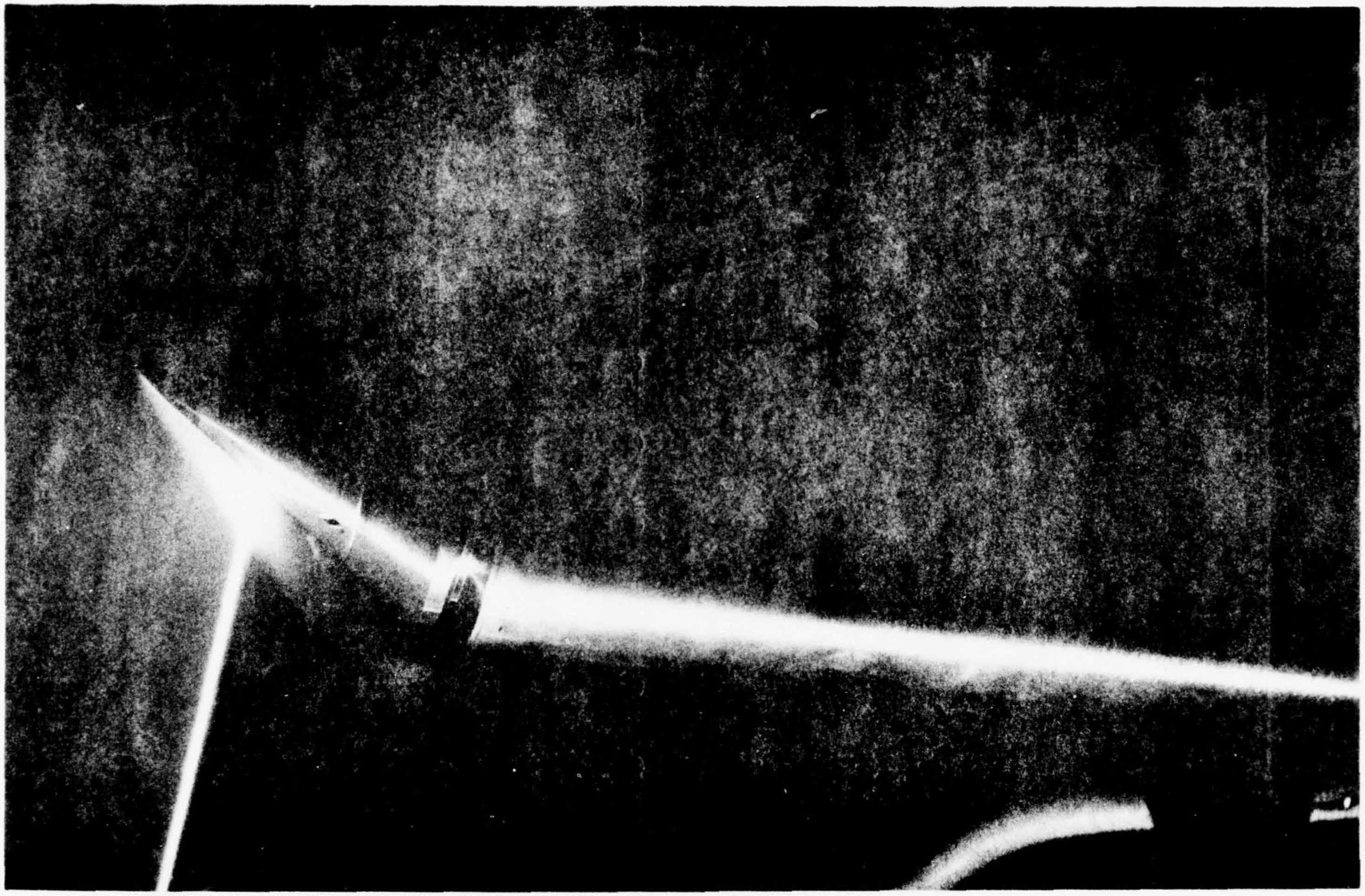

Figure 22. Electron Beam Flow Visualization Photograph of Full Scale Aspirated Model in AEDC Chamber 10v

Photo 621 - $\alpha=+5^{O}$, $P_{O}=.45$ torr, $T_{O}=350^{O}K$, 79 Km altitude

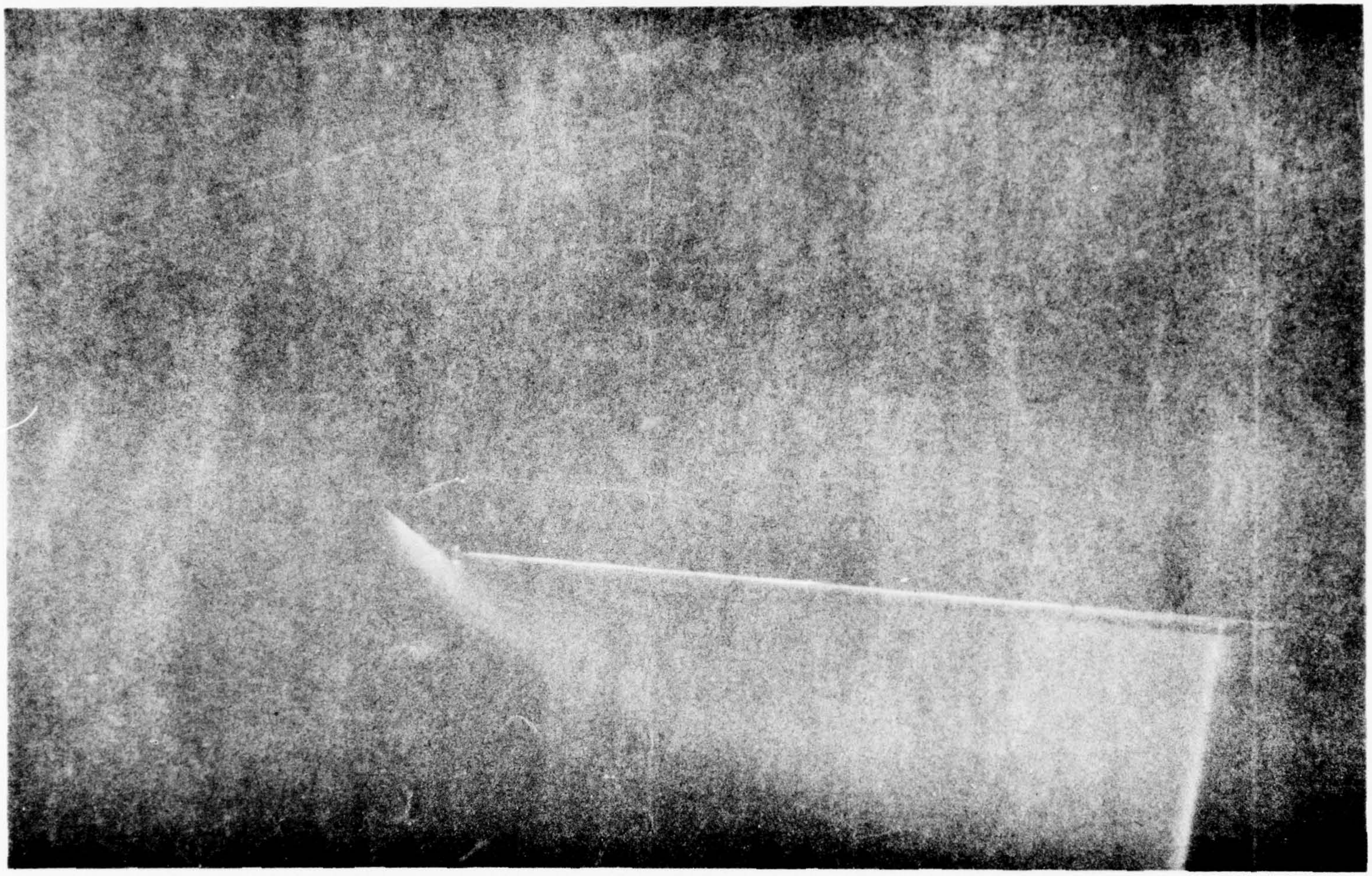

Figure 23. Electron Beam Flow Visualization Photograph of 1/10 Scale Model in AEDC Chamber 10v

Photo 871 - $\alpha=+5^{o}$, $P_{o}=.45$ torr, $T_{o}=260^{o}K$, 77.5 Km altitude

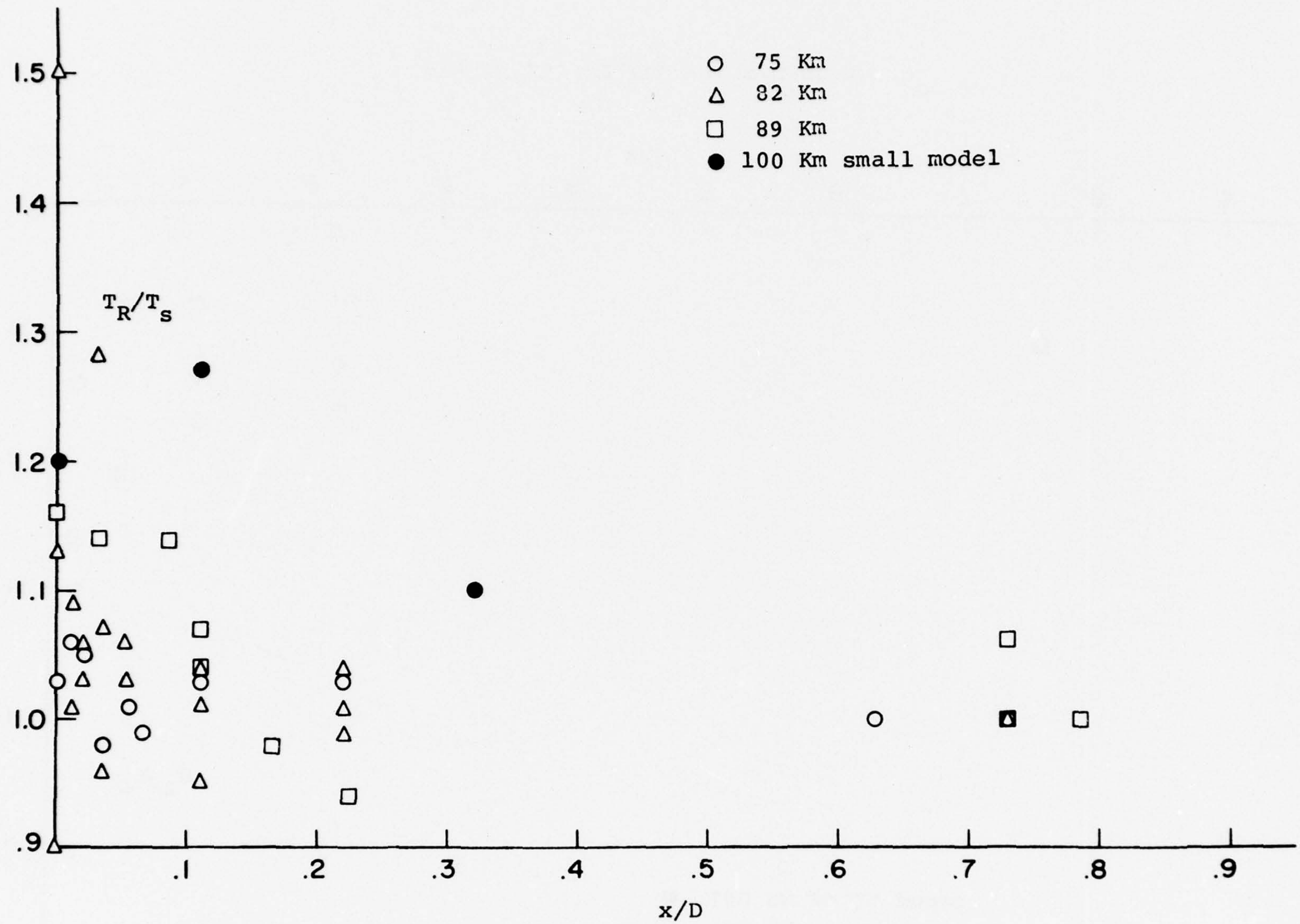

Figure 24. T_R/T_s vs. x/D at $\alpha = 0^{\circ}$

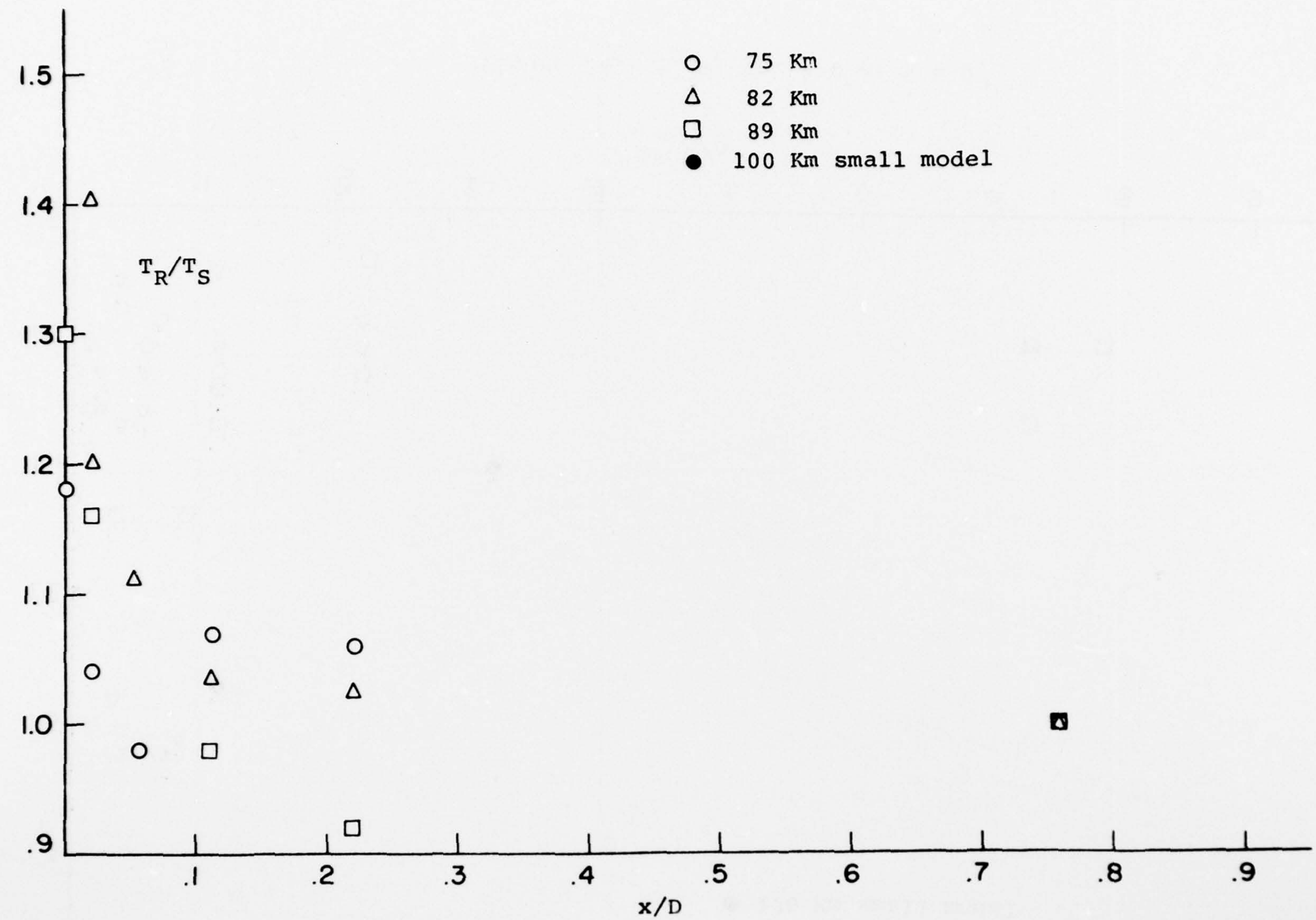

Figure 25. T_R/T_S vs. x/D at $\alpha = 5^{\circ}$

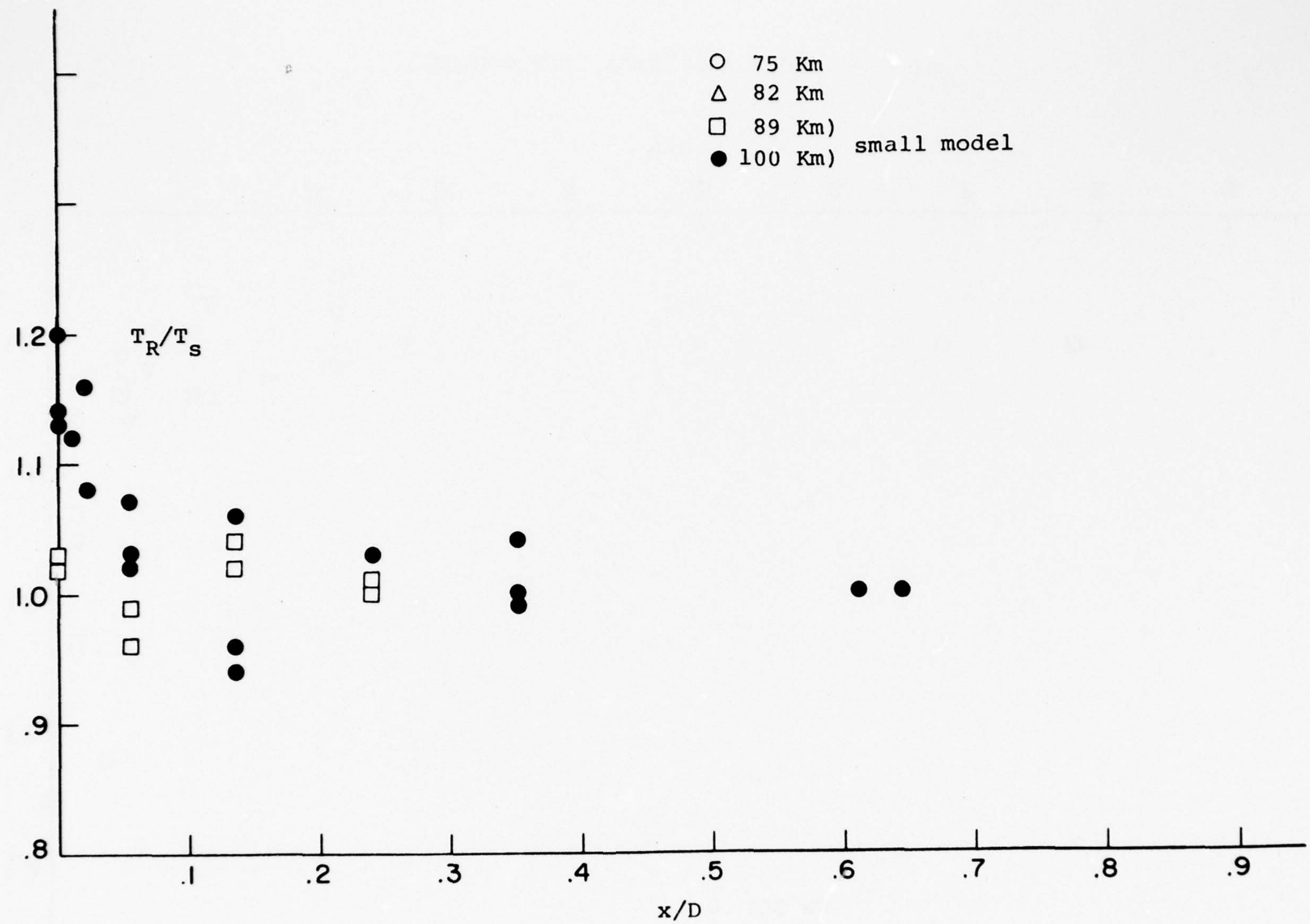

Figure 26. T_R/T_s vs. x/D at $\alpha = 5.5^o$

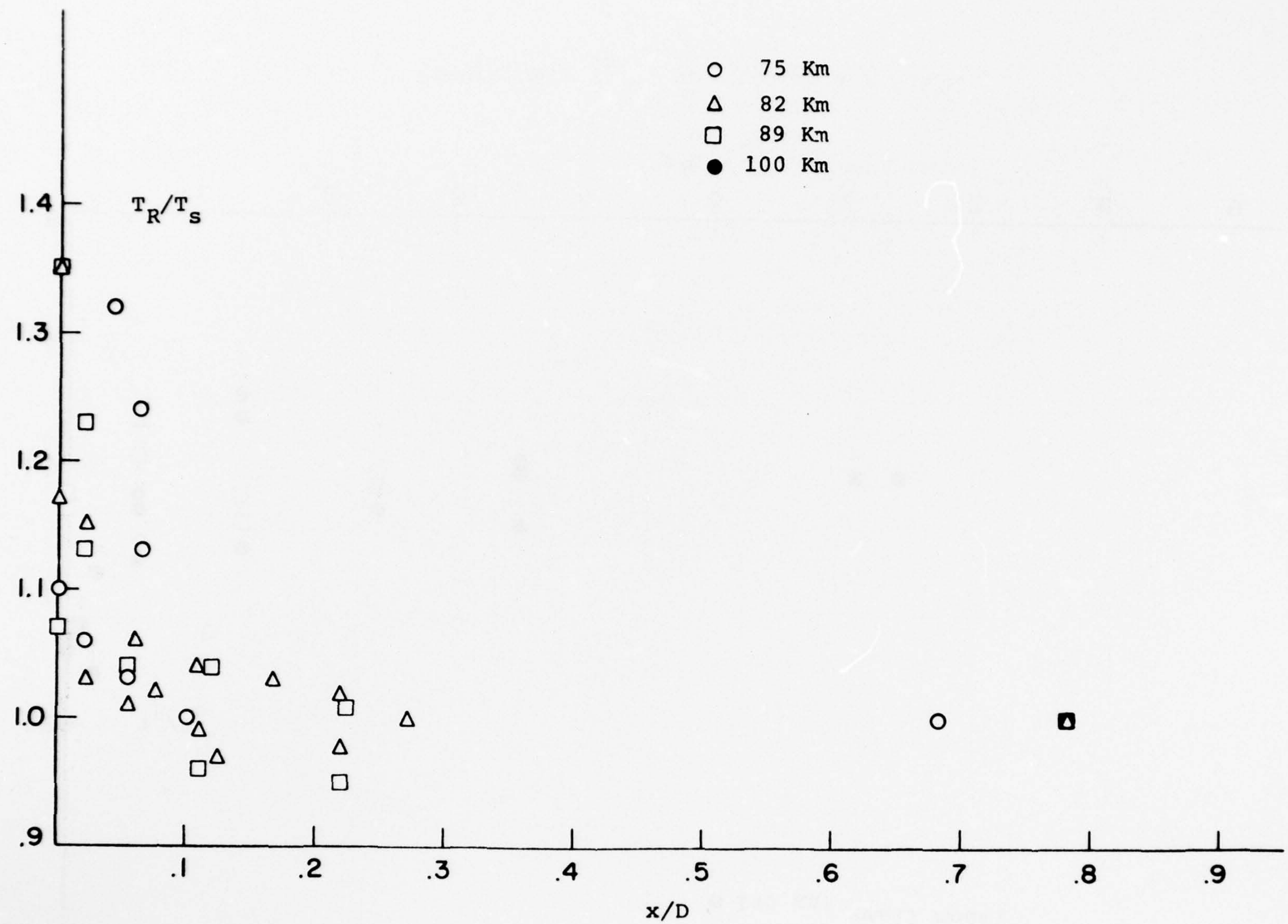

Figure 27. T_R/T_s vs. x/D at $\alpha = 10^o$

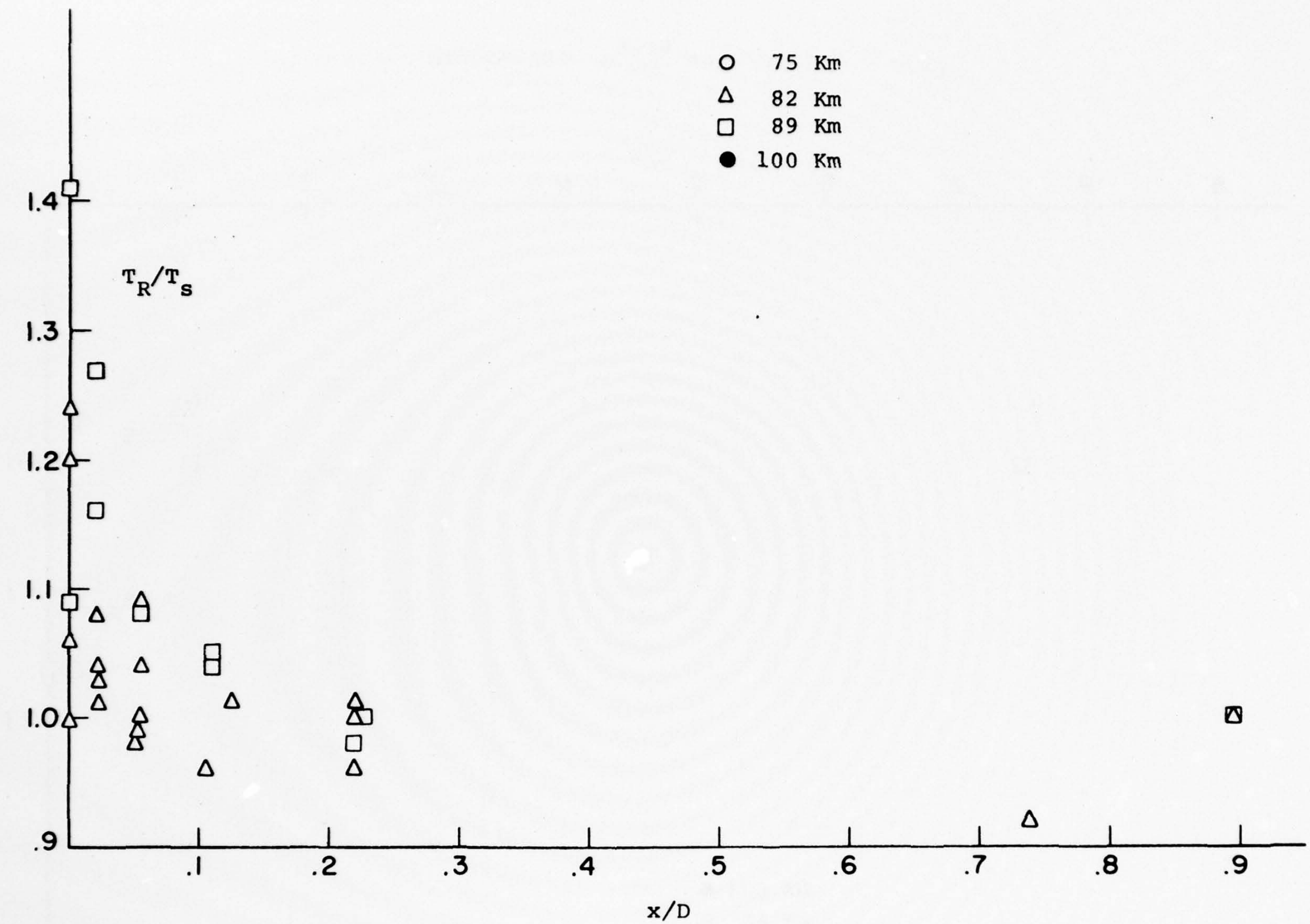

Figure 28. T_R/T_s vs x/D at $\alpha = 20^{\circ}$

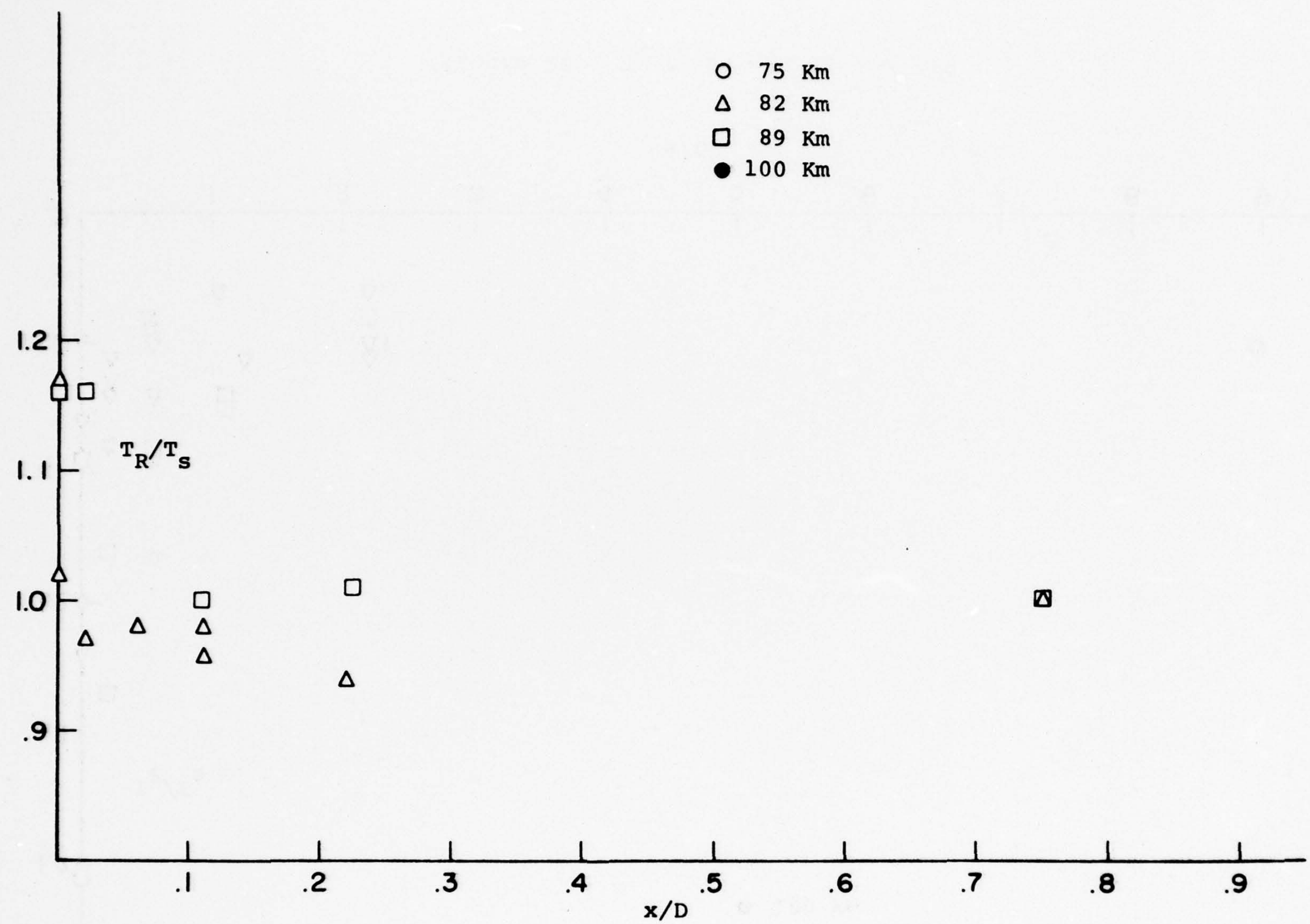

Figure 29. T_R/T_s vs x/D at $\alpha = -10^o$

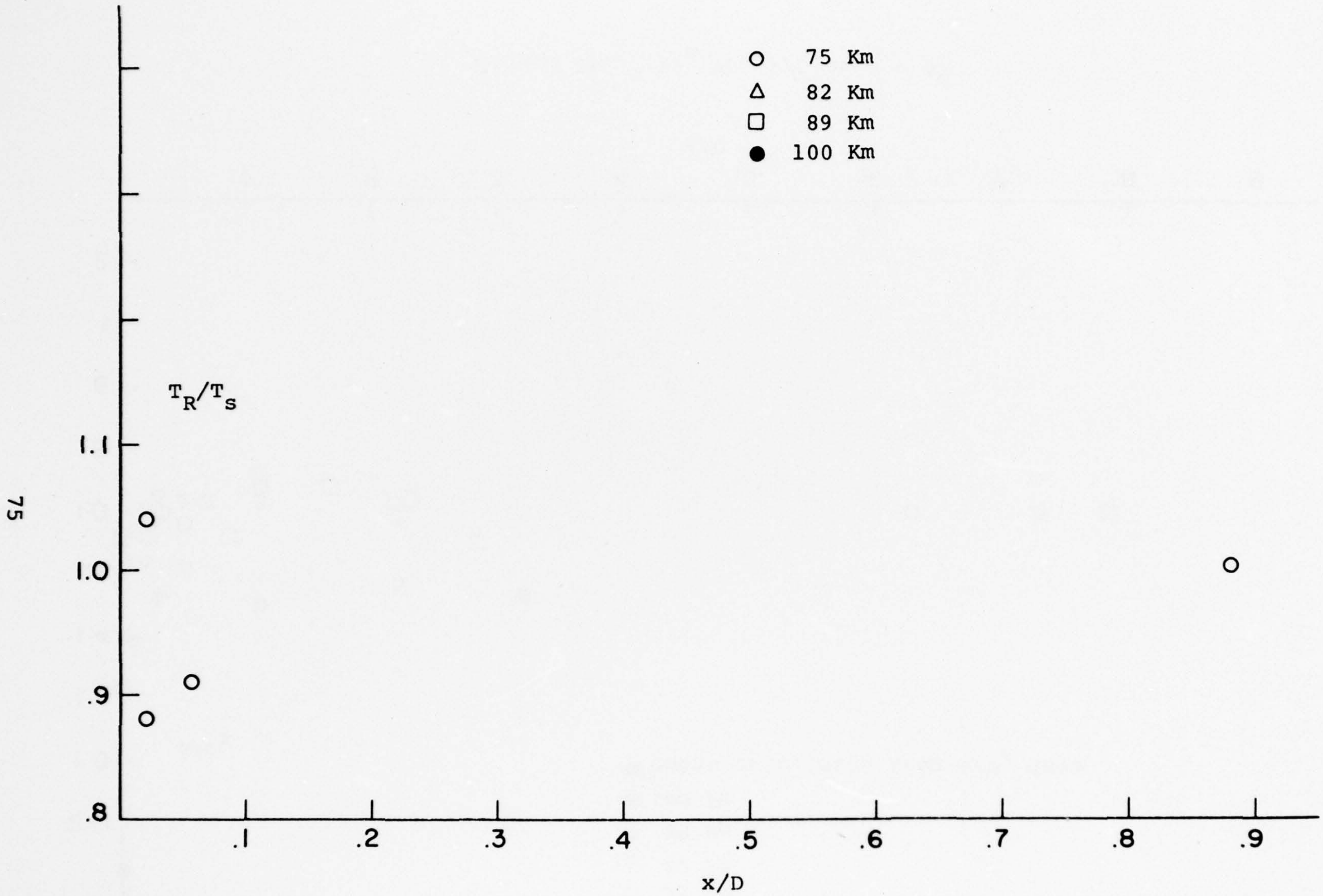

Figure 30. T_R/T_s vs. x/D at $\alpha = -20^{\circ}$

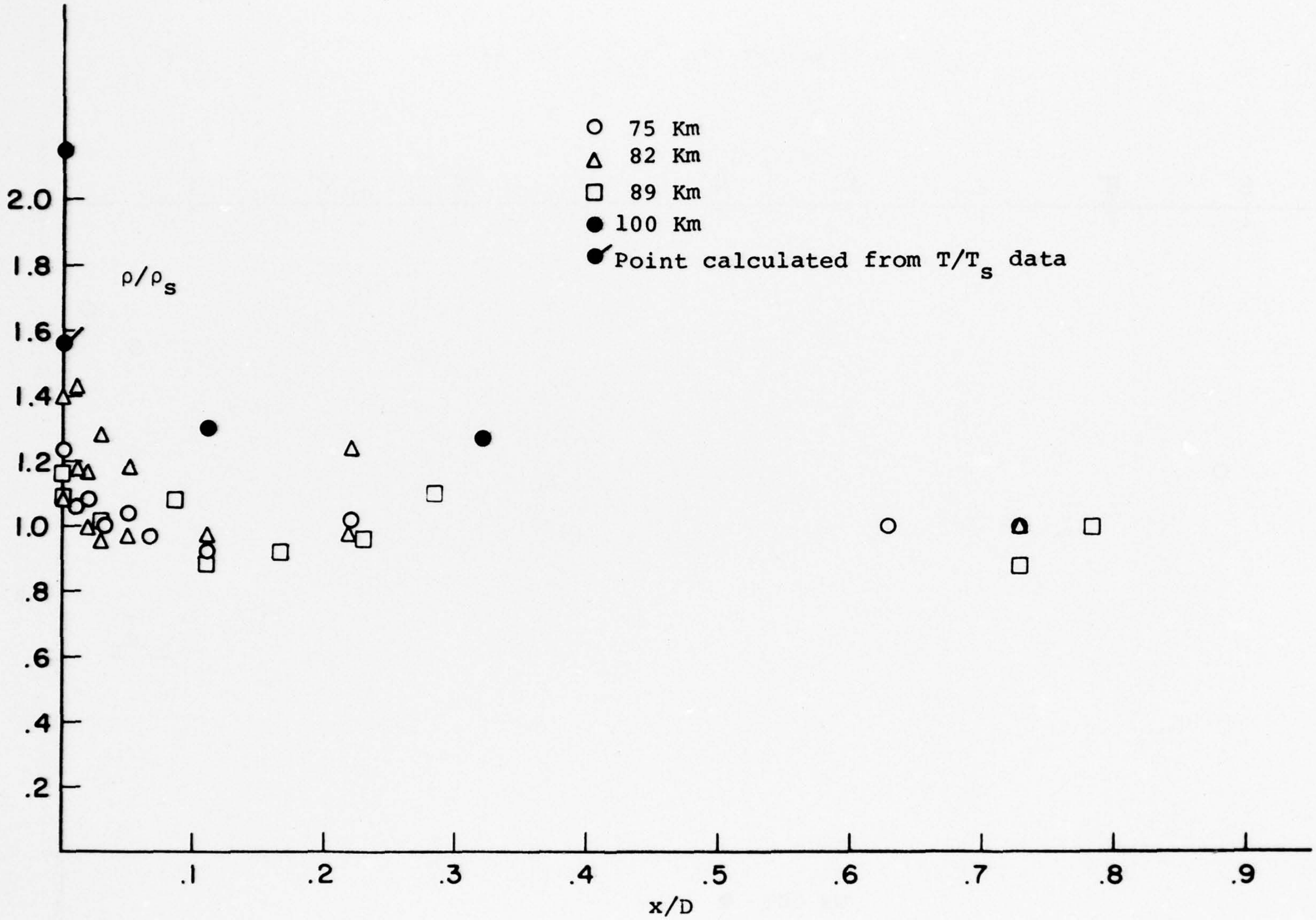

Figure 31. ρ/ρ_s vs. x/D at $\alpha = 0^o$

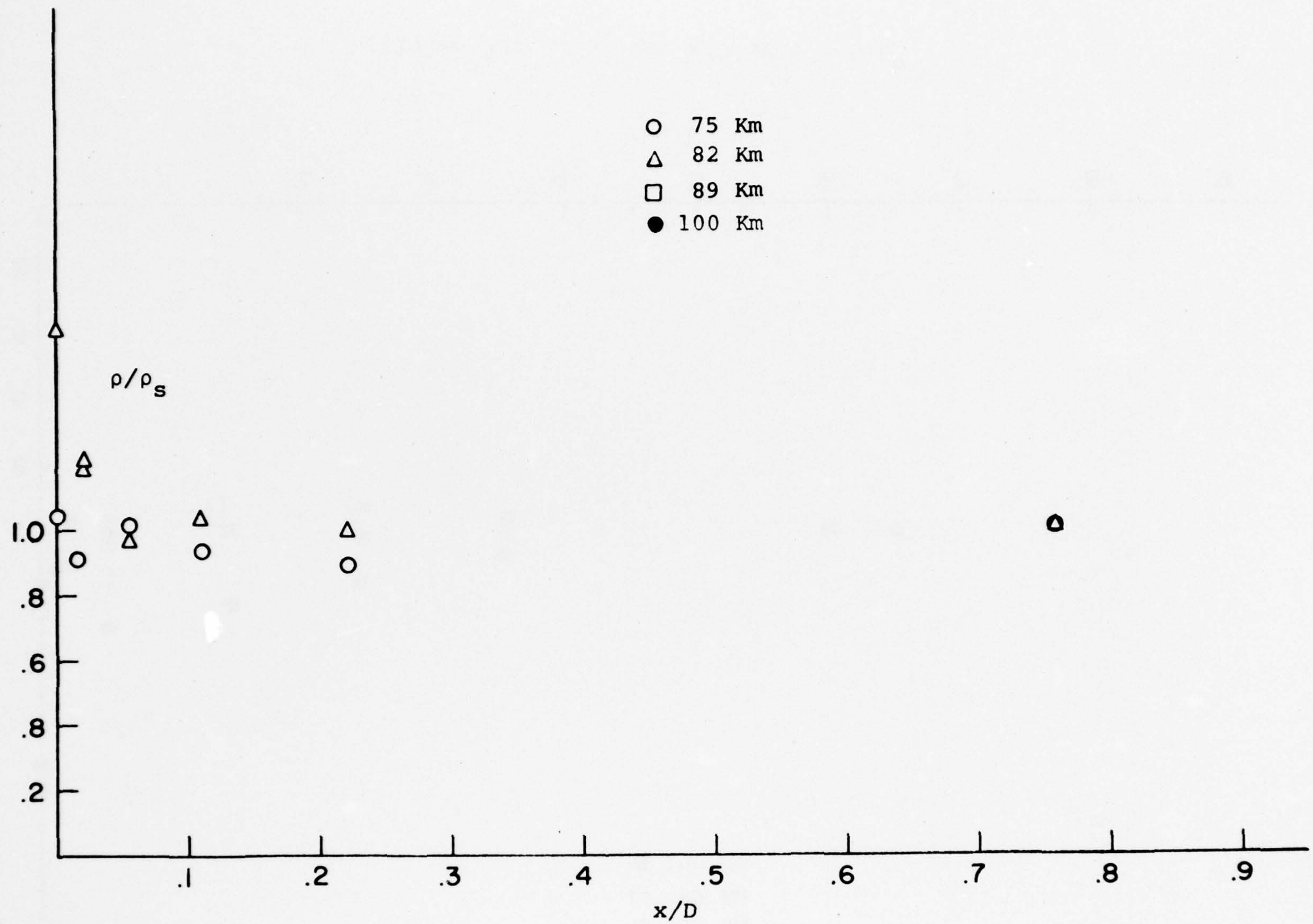

Figure 32. ρ/ρ_s vs. x/D at $\alpha = 5^{\circ}$

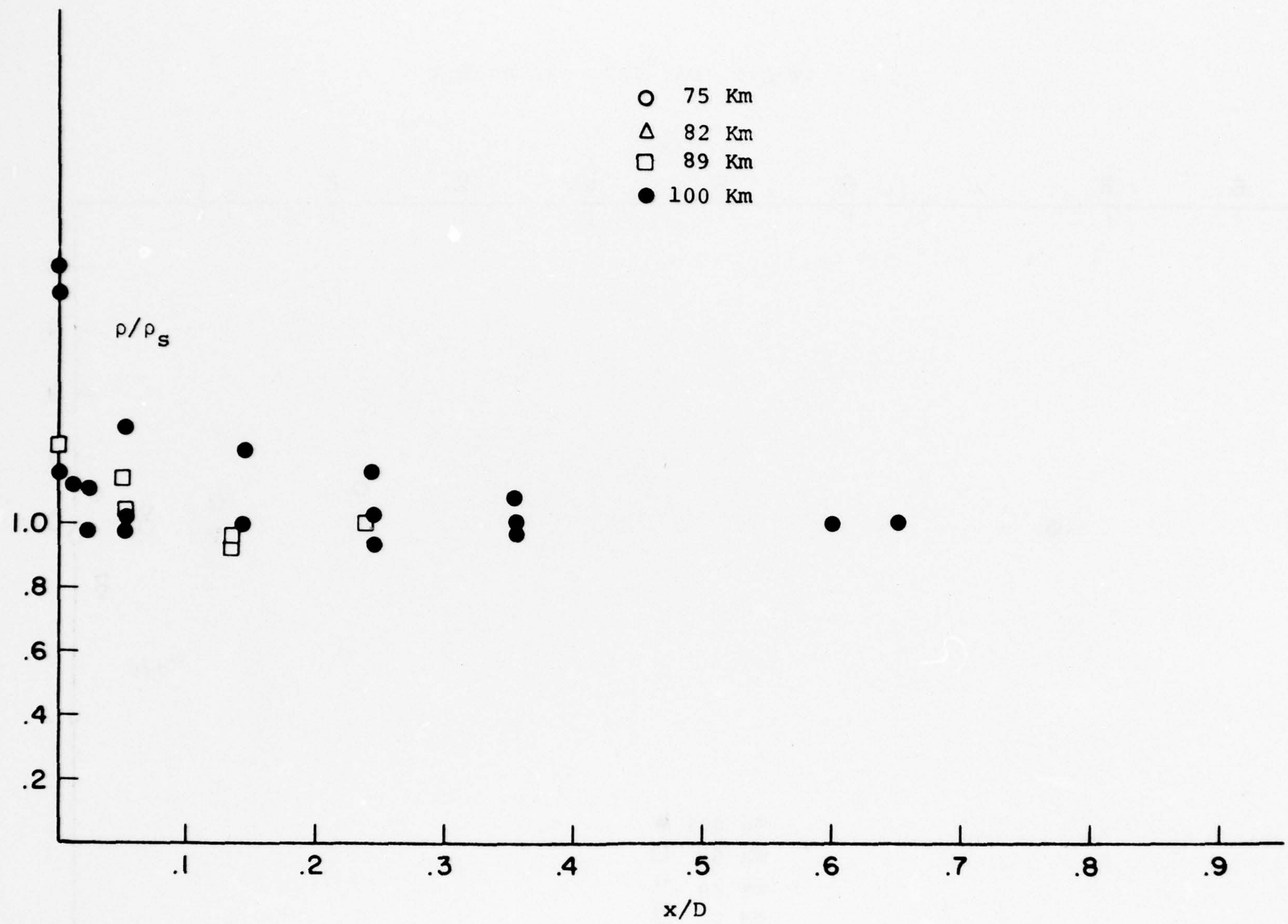

Figure 33. ρ/ρ_s vs. x/D at $\alpha = 5.5^{\circ}$

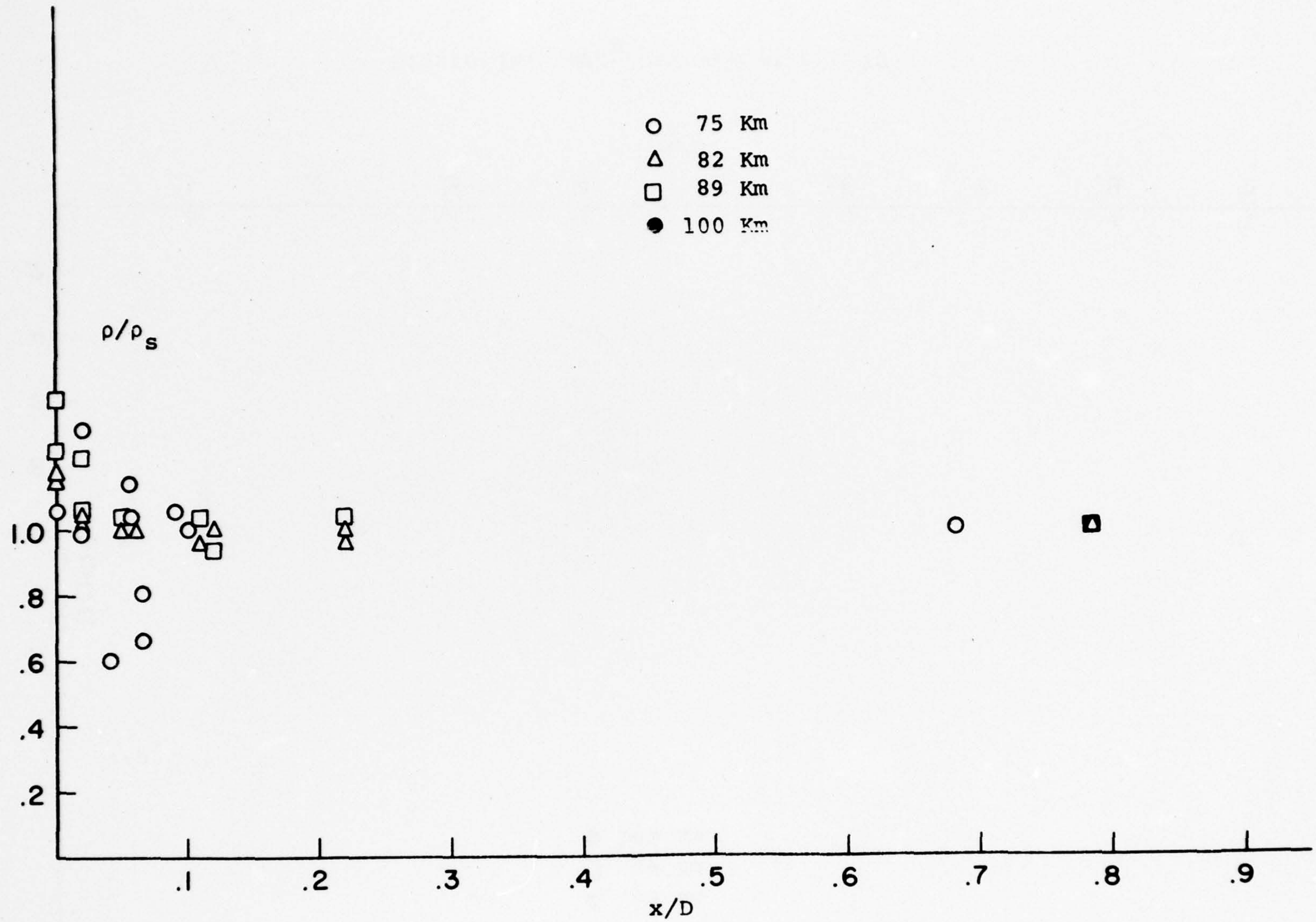

Figure 34. ρ/ρ_s vs. x/D at $\alpha = 10^0$

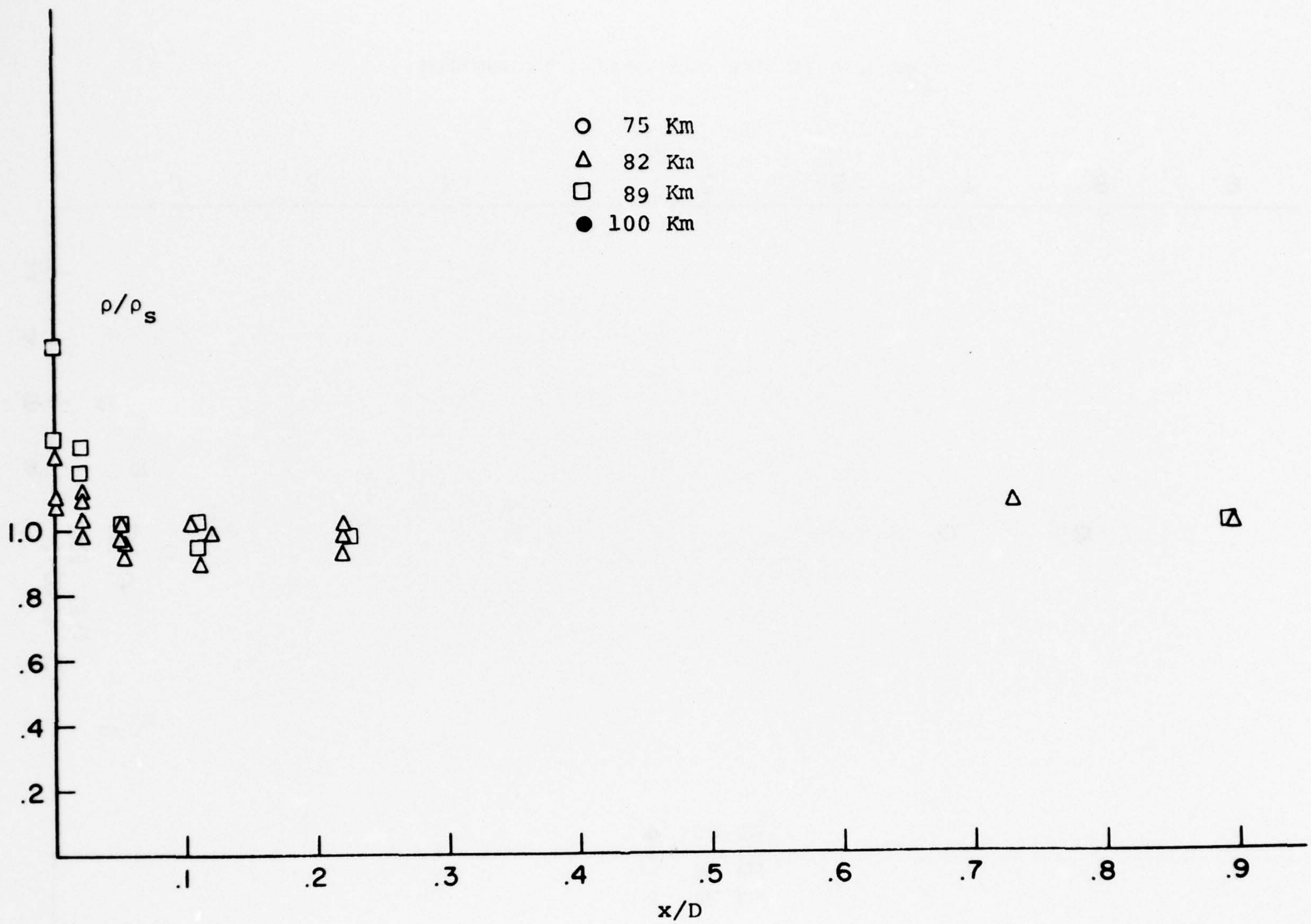

Figure 35. ρ/ρ_s vs. x/D at $\alpha = 20^{\circ}$

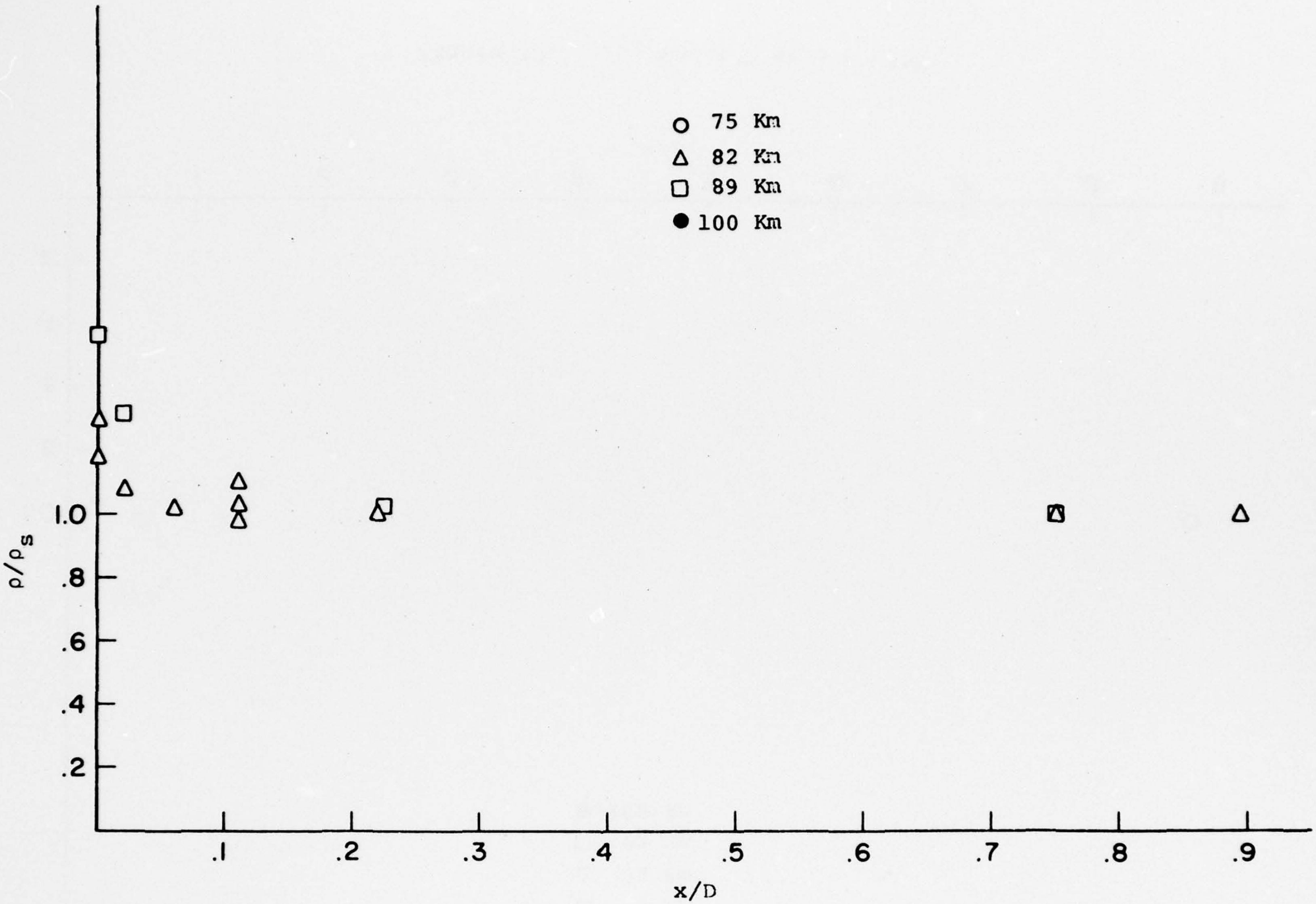

Figure 36. ρ/ρ_s vs. x/D at $\alpha = -10^{\circ}$

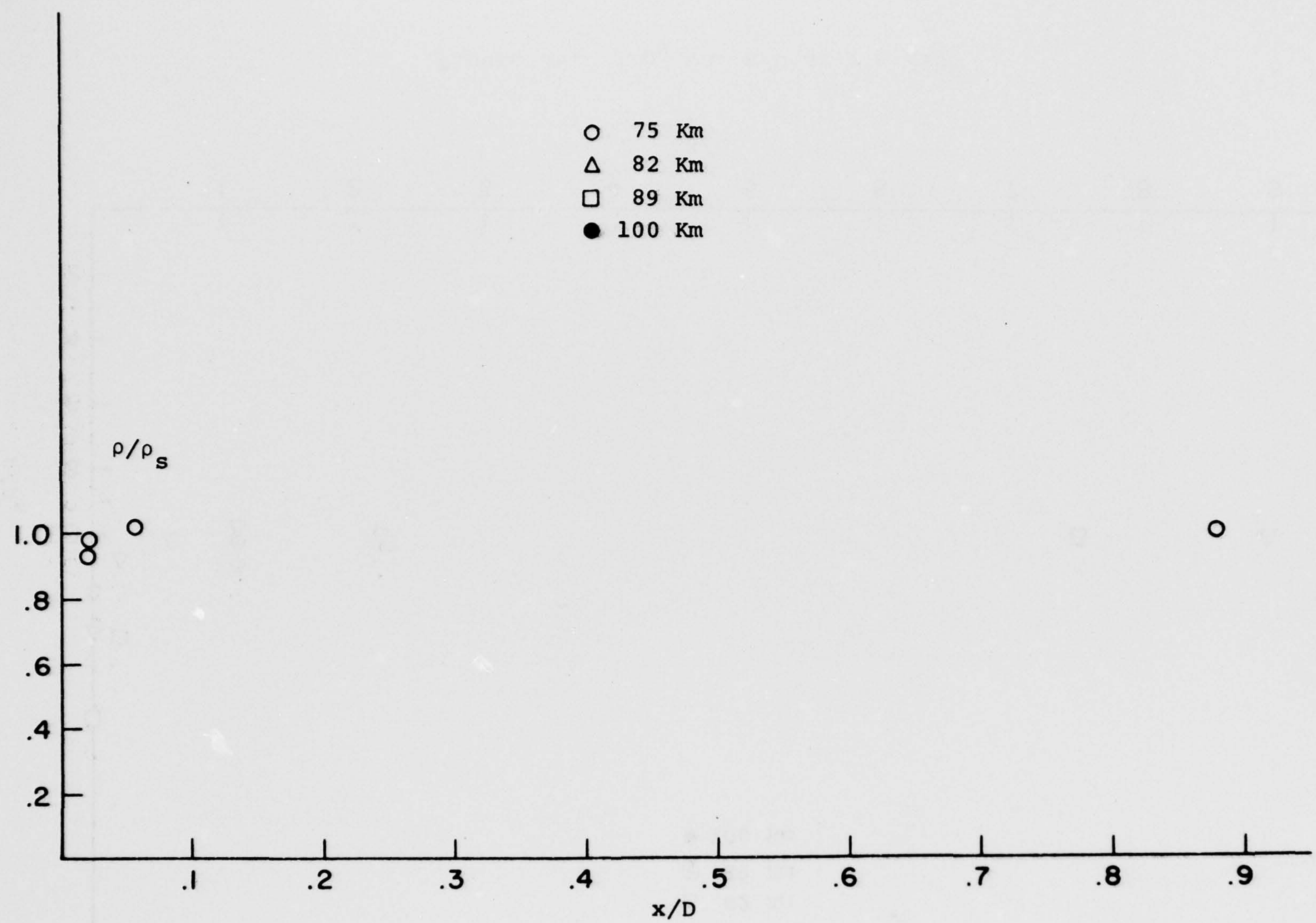

Figure 37. ρ/ρ_s vs. x/D at $\alpha = -20^{\circ}$

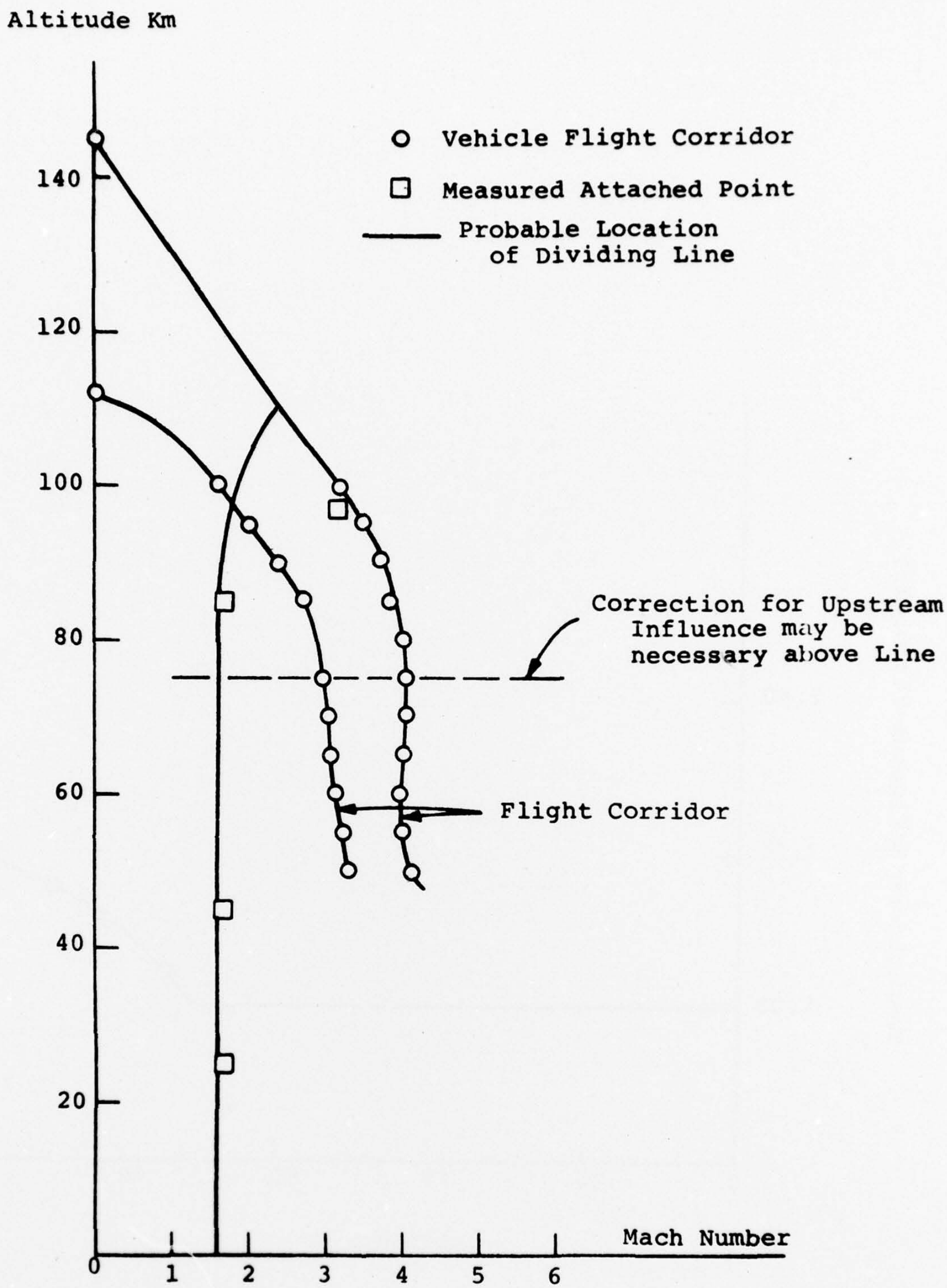

Figure 38. Region for Attached Shock for 35° Conical Skimmer

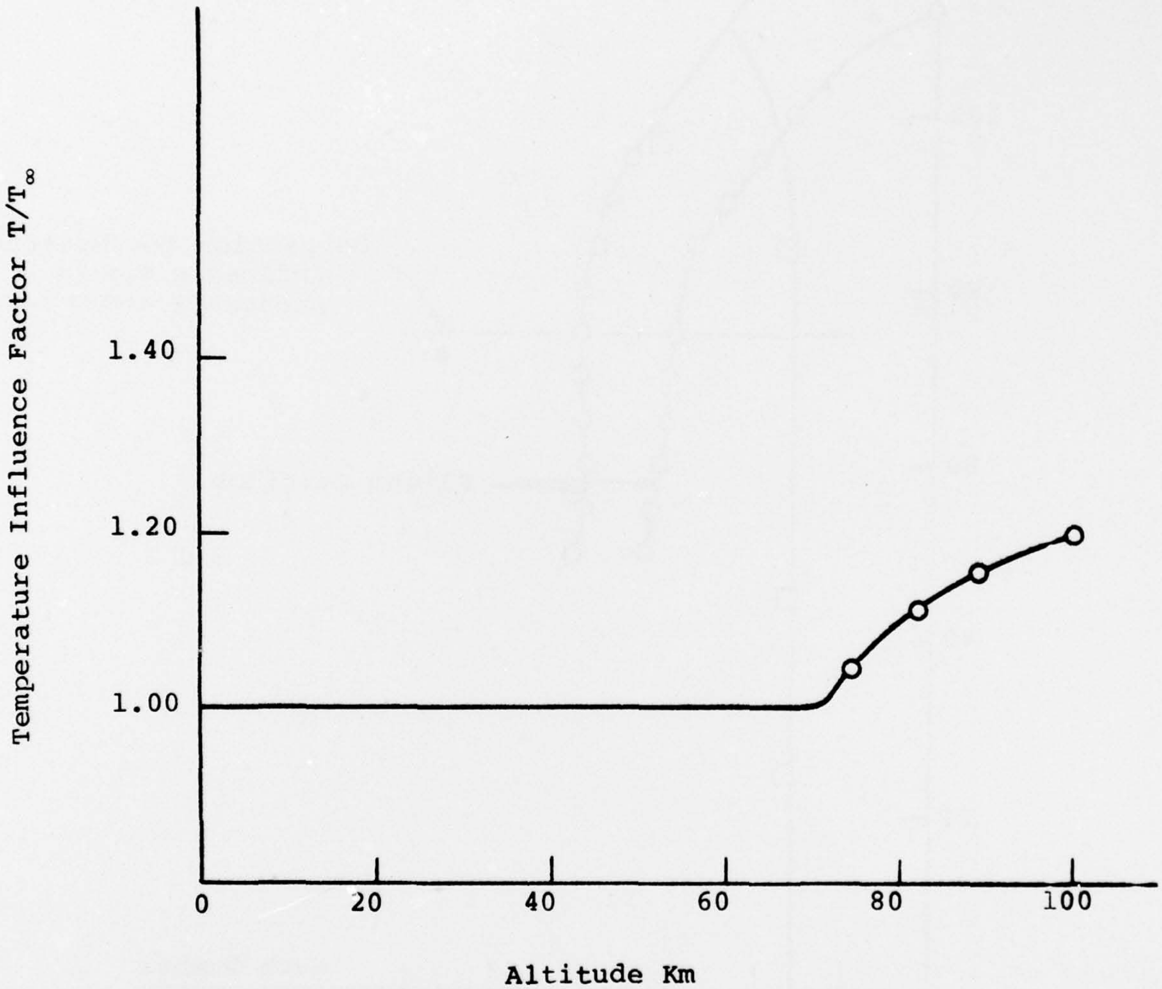

Figure 39. Temperature Influence Factor for Upstream Influence at M=3-4 from AEDC Tests of 35° Conical Skimmer

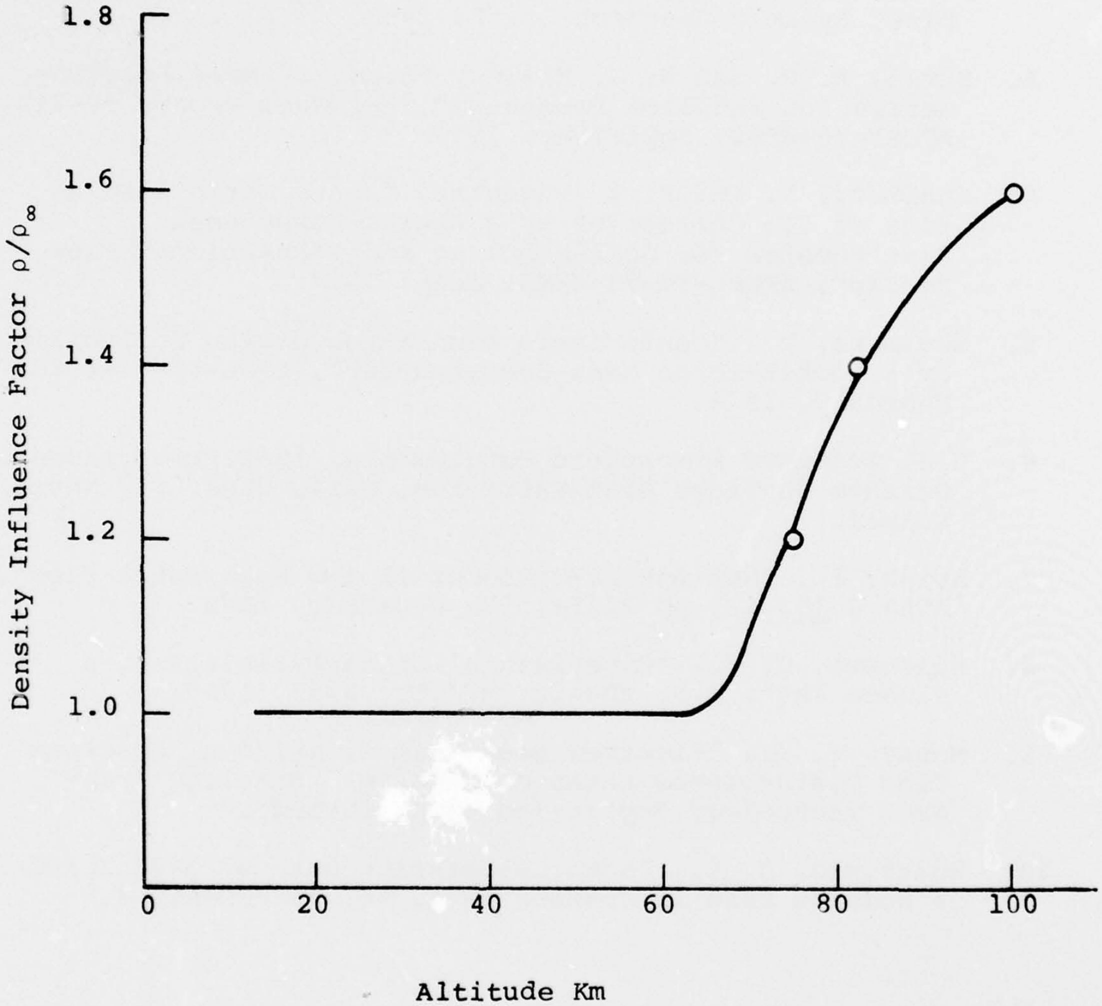

Figure 40. Density Influence Factor for Upstream Influence at M=3-4 from AEDC Tests of 35° Conical Skimmer

REFERENCES

1. Narcisi, R. S. and A. D. Bailey, "Mass Spectrometric Measurements of Positive Ions at Altitudes from 64 to 112 Kilometers", J. Geophys. Res. 70, 3687-3700 (1965).

2. "National Advisory Committee for Aeronautics, Report 1135, "Equations, Tables, and Charts for Compressible Flow" by Ames Research Staff, 1953.

3. Burke, R. R. and W. J. Miller, "Study of Mass Spectrometric Ion Sampling Processes", AeroChem Report TP-247, AFCRL-70-0550, September, 1970.

4. Sugimura, T. and F. W. Vogenitz, "Monte Carlo Simulation of Ion Collection by a Rocket-Borne Mass Spectrometer for Collisionless and Transitional Flow Fields", AFCRL-TR-73-0448, July, 1973.

5. Sugimura, T., "Monte Carlo Simulation of Ion Collection by a Rocket-Borne Mass Spectrometer", AFGL-TR-76-0029, February, 1976.

6. U.S. Standard Atmosphere Supplements, 1966, Environmental Science Services Administration, NASA, USAF, 15^{o} North Annual.

7. Hsieh, T., "Hemisphere-Cylinder in Low Supersonic Flow", AIAA J 13, 12, pp 1551-1552, December, 1975.

8. Haldeman, C. W., "Experimental Characteristics of a Plasma Jet", M.S. thesis, M.I.T., June, 1959.

9. McKay, T. D., "Electron Beam Investigation of Upstream Flow Disturbances Ahead of a Conical Sampling Probe", AEDC Technology Report (to be published).

10. Whitfield, D. L., "Some Calibration Data of Mach 3 and 6 Nozzles used in Chamber 10V", No. VKF/LR-ASP-3.